

An Effective Model of the Retinoic Acid Induced HL-60 Differentiation Program

Ryan Tasseff, Holly A. Jensen, Wei Dai, Katherine Rogers, Adithya Sagar, Rodica P. Bunaciu[†], Johanna Congleton[†], Andrew Yen[†], and Jeffrey D. Varner*

Robert Frederick Smith School of Chemical and Biomolecular Engineering and [†]Department of Biomedical Sciences, Cornell University, Ithaca NY 14853

Running Title: Effective modeling of HL-60 differentiation

To be submitted: *Frontiers in Systems Biology*

*Corresponding author:

Jeffrey D. Varner,

Professor, Robert Frederick Smith School of Chemical and Biomolecular Engineering,
244 Olin Hall, Cornell University, Ithaca NY, 14853

Email: jdv27@cornell.edu

Phone: (607) 255 - 4258

Fax: (607) 255 - 9166

Abstract

In this study, we present an effective model All-Trans Retinoic Acid (ATRA)-induced differentiation of HL-60 cells. The model describes a key architectural feature of ATRA-induced differentiation, positive feedback between an ATRA-inducible signalsome complex involving many proteins including Vav1, a guanine nucleotide exchange factor, and the activation of the mitogen activated protein kinase (MAPK) cascade. The model, which was developed by integrating logical rules with kinetic modeling, was significantly smaller than previous models. However, despite its simplicity, it captured key features of ATRA induced differentiation of HL-60 cells. We identified an ensemble of effective model parameters using measurements taken from ATRA-induced HL-60 cells. Using these parameters, model analysis predicted that MAPK activation was bistable as a function of ATRA exposure. Conformational experiments supported ATRA-induced bistability. These findings, combined with other literature evidence, suggest that positive feedback is central to a diversity of cell fate programs.

1 Introduction

2 Understanding the architecture of differentiation programs is an important therapeutic
3 challenge. Differentiation induction chemotherapy (DIC), using agents such as the vita-
4 min A derivative all-trans retinoic acid (ATRA), is a promising approach for the treatment
5 of many cancers (1–3). For example, ATRA treatment induces remission in 80–90% of
6 promyelocytic leukemia (APL) PML-RAR α -positive patients (4), thereby transforming a
7 fatal diagnosis into a manageable disease. However, remission is sometimes not durable
8 and relapsed cases exhibit emergent ATRA resistance (5, 6). To understand the basis of
9 this resistance, we must first understand the ATRA-induced differentiation program. To-
10 ward this challenge, lessons learned in model systems, such as the lineage-uncommitted
11 human myeloblastic cell line HL-60, could inform our analysis of the more complex dif-
12 ferentiation programs occurring in patients. Patient derived HL-60 leukemia cells have
13 been a durable experimental model since the 1970's to study differentiation (7). HL-60
14 undergoes cell cycle arrest and either myeloid or monocytic differentiation following stim-
15 ulation; ATRA induces G1/G0-arrest and myeloid differentiation in HL-60 cells, while 1,25-
16 dihydroxy vitamin D3 (D3) induces arrest and monocytic differentiation. Commitment to
17 cell cycle arrest and differentiation requires approximately 48 hr of treatment, during which
18 HL-60 cells undergo two division cycles.

19 Sustained mitogen-activated protein kinase (MAPK) activation is a defining feature of
20 ATRA-induced HL-60 differentiation. ATRA drives sustained MEK-dependent activation
21 of the Raf/MEK/ERK pathway, leading to arrest and differentiation (8). MEK inhibition re-
22 sults in the loss of ERK and Raf phosphorylation, and the failure to arrest and differentiate
23 (9). ATRA (and its metabolites) are ligands for the hormone activated nuclear transcrip-
24 tion factors retinoic acid receptor (RAR) and retinoid X receptor (RXR) (10). RAR/RXR
25 activation is necessary for ATRA-induced Raf phosphorylation (9), and the formation of
26 an ATRA-inducible signalsome complex at the membrane which drives MAPK activation

27 through a yet to be identified kinase activity. While the makeup of the signalsome com-
28 plex is not yet known, we do know that it is composed of Src family kinases Fgr and Lyn,
29 PI3K, c-Cbl, Slp76, and KSR, as well as IRF-1 transcription factors (11–15). Signalsome
30 formation and activity is driven by ATRA-induced expression of CD38 and the putative
31 heterotrimeric Gq protein-coupled receptor BLR1 (16, 17). BLR1, identified as an early
32 ATRA (or D3)-inducible gene using differential display (18), is necessary for MAPK ac-
33 tivation and differentiation (17), and is also involved with signalsome activity. Studies
34 of the BLR1 promoter identified a 5' 17bp GT box approximately 1 kb upstream of the
35 transcriptional start that conferred ATRA responsiveness (17). Members of the BLR1
36 transcriptional activator complex, e.g. NFATc3 and CREB, are phosphorylated by ERK,
37 JNK or p38 MAPK family members suggesting positive feedback between the signalsome
38 and MAPK activation (19). BLR1 overexpression enhanced Raf phosphorylation and ac-
39 celerated terminal differentiation, while Raf inhibition reduced BLR1 expression and dif-
40 ferentiation (20). BLR1 knock-out cells failed to activate Raf or differentiate in the pres-
41 ence of ATRA (20). Interestingly, both the knockdown or inhibition of Raf, also reduced
42 BLR1 expression and functional differentiation (20). Thus, the expression of signalsome
43 components e.g., BLR1 was Raf dependent, while Raf activation depended upon the sig-
44 nalsome. A recent computational study of ATRA-induced differentiation in HL-60 cells
45 suggested that the BLR1-MAPK positive feedback circuit was sufficient to explain ATRA-
46 induced sustained MAPK activation, and the expression of a limited number of functional
47 differentiation markers (21). Model analysis also suggested that Raf was the most distinct
48 of the MAPK proteins. However, this previous study developed and analyzed a complex
49 model, thus leaving open the critical question of what is the minimal positive feedback
50 circuit required to drive ATRA-induced differentiation.

51 In this study, we explored this question using a minimal mathematical model of the
52 key architectural feature of ATRA induced differentiation of HL-60 cells, namely positive

53 feedback between an ATRA-inducible signalsome complex and MAPK activation. The
54 ATRA responsive signalsome-MAPK circuit was then used to drive a downstream gene
55 expression program which encoded for the expression of functional differentiation mark-
56 ers. The effective model used a novel framework which integrated logical rules with ki-
57 netic modeling to describe gene expression and protein regulation, while largely relying
58 upon biophysical parameters from the literature. This formulation significantly reduced
59 the size and complexity of the model compared to the previous study of Tasseff et al.,
60 while increasing the breadth of the biology described (21). The effective model, despite
61 its simplicity, captured key features of ATRA induced differentiation of HL-60 cells. Model
62 analysis predicted the bistability of MAPK activation as a function of ATRA exposure; con-
63 formational experiments supported ATRA-induced bistability. Model simulations were also
64 consistent with measurements of the influence of MAPK inhibitors, and the failure of BLR1
65 knockout cells to differentiate when exposed to ATRA. Lastly, we showed by through im-
66 munoprecipitation studies, that the guanine nucleotide exchange factor Vav1 is potentially
67 a new ATRA-inducible member of the signalsome complex. Taken together, these findings
68 when combined with other literature evidence, suggested that positive feedback architec-
69 tures are central to differentiation programs generally, and necessary for ATRA-induced
70 differentiation.

71 **Results**

72 We constructed an effective model of ATRA-induced HL-60 differentiation which described
73 signaling and gene expression events following the addition of ATRA (Fig. 1). The model
74 connectivity was developed from literature and the studies presented here (Table 1). We
75 decomposed the ATRA program into three modules; a signal initiation module that sensed
76 and transformed the ATRA signal into activated cRaf-pS621 and the ATRA-RXR/RAR
77 (Trigger) signals (Fig. 1A); a signal integration module that controlled the expression of
78 upstream transcription factors given cRaf-pS621 and activated Trigger signals (Fig. 1B);
79 and a phenotype module which encoded the expression of functional differentiation mark-
80 ers from the ATRA-inducible transcription factors (Fig. 1C). Each component of these
81 modules was described by a mRNA and protein balance equation. Additionally, the sig-
82 nal initiation module also described the abundance of activated species e.g., Trigger and
83 cRaf-pS621 whose values were derived from unactivated Trigger and cRaf protein levels.
84 Lastly, because the population of HL-60 cells was dividing (at least before ATRA-induced
85 cell cycle arrest), we also considered a dilution term in all balance equations. The sig-
86 nal initiation module contained nine differential equations, while the signal integration and
87 phenotype modules were collectively encoded by 54 differential equations. Model param-
88 eters were taken literature (Table 2), or estimated from experimental data using heuristic
89 optimization (see materials and methods).

90 The signal initiation module recapitulated sustained signalsome and MAPK activation
91 following exposure to $1\mu\text{M}$ ATRA (Fig. 2A-B). An ensemble of effective model param-
92 eters was estimated by minimizing the difference between simulations and time-series
93 measurements of BLR1 mRNA and cRaf-pS621 following the addition of $1\mu\text{M}$ ATRA. We
94 focused on the S621 phosphorylation site of cRaf since enhanced phosphorylation at
95 this site is a defining characteristic of sustained MAPK activation in HL-60. The effective
96 model captured both ATRA-induced BLR1 expression (Fig. 2A) and sustained phospho-

97 phosphorylation of cRaf-pS621 (Fig. 2B) in a growing population of HL-60 cells. Together, the
98 reinforcing positive feedback between the signalsome and MAPK led to sustained activation
99 over multiple cellular generations. However, the effective model failed to capture the
100 decline of BLR1 message after 48 hr of ATRA exposure. This suggested that we captured
101 the logic leading to the onset of differentiation, but failed to describe program shutdown.
102 Next, we tested the response of the signal initiation module to different ATRA dosages.

103 The signal initiation model was bistable with respect to ATRA induction (Fig. 2C-D).
104 Phaseplane analysis predicted two stable steady-states when ATRA was present below
105 a critical threshold, and only a single steady-state above the threshold (Fig. 2C). In the
106 lower stable state, neither the signalsome nor cRaf-pS621 were present (thus, the differ-
107 entiation program was deactivated). However, at the high stable state, both the signal-
108 some and cRaf-pS621 were present, allowing for sustained activation and differentiation.
109 Interestingly, when ATRA was above a critical threshold, only the activated state was ac-
110 cessible (Fig. 2D). To test these findings, we first identified the ATRA threshold. We
111 exposed HL-60 cells to different ATRA concentrations for 72 hr (Fig. 2E). Morphological
112 changes associated with differentiation were visible for ATRA \geq 0.25 μ M, suggesting the
113 critical ATRA threshold was near this concentration. Next, we conducted ATRA washout
114 experiments to determine if activated cells remained activated in the absence of ATRA.
115 HL-60 cells locked into an activated state remained activated following ATRA withdraw-
116 (Fig. 3). This sustained activation resulted from reinforcing feedback between the sig-
117 nalsome and the MAPK pathway. Thus, following activation, if we inhibited or removed
118 elements from the signal initiation module we expected the signalsome and MAPK signals
119 to decay. We simulated ATRA induced activation in the presence of kinase inhibitors, and
120 without key circuit elements. Consistent with experimental results using multiple MAPK
121 inhibitors, ATRA activation in the presence of MAPK inhibitors lowered the steady-state
122 value of signalsome (Fig. 3A). In the presence of BLR1, the signalsome and cRaf-pS621

123 signals were maintained following ATRA withdraw (Fig. 3B, gray). On the other hand,
124 BLR1 deletion removed the ability of the circuit to maintain a sustained MAPK response
125 following the withdraw of ATRA (Fig. 3B, blue). Lastly, washout experiments in which
126 cells were exposed to $1\mu\text{M}$ ATRA for 24 hr, and then transferred to fresh media with-
127 out ATRA, confirmed the persistence of the self sustaining activated state for up to 144
128 hr (Fig. 3C). Thus, these experiments confirmed that reinforcing positive feedback likely
129 drives the ATRA-induced differentiation program. Next, we analyzed the ATRA-induced
130 downstream gene expression program following signalsome and cRaf activation.

131 The signal integration and phenotype modules described ATRA-induced gene expres-
132 sion in wild-type HL-60 cells (Fig. 4). The signal initiation module produced two outputs,
133 activated Trigger and cRaf-pS621 which drove the expression of ATRA-induced transcrip-
134 tion factors, which then in turn activated the phenotypic program. In particular, Trigger,
135 which is a surrogate for the RAR α /RXR transcriptional complex, regulated the expres-
136 sion of the transcription factors CCATT/enhancer binding protein α (C/EBP α), PU.1, and
137 EGR1. In turn, these transcription factors, in combination with cRaf-pS621, regulated the
138 expression of downstream phenotypic markers such as CD38, CD11b or P47Phox. We
139 assembled the connectivity of the signal integration and phenotypic programs driven by
140 Trigger and cRaf-pS621 from literature (Table 1). We estimated the parameters which
141 appeared in the control laws regulating these programs from steady-state and dynamic
142 measurements of transcription factor and phenotypic marker expression following the ad-
143 dition of ATRA (22–25). However, the bulk of the remaining model parameters were taken
144 from directly from literature (26) and were not estimated in this study (see materials and
145 methods). The model simulations captured the time dependent expression of CD38 and
146 CD11b following the addition ATRA (Fig. 4A), and the steady-state for signal integration
147 and phenotypic markers (Fig. 4B). Lastly, we used the *predicted* values of the p21 and
148 E2F protein abundance to estimate a blackbox model of ATRA-induced G0 arrest (Fig.

149 5). The phenotype module predicted p21 expression significantly increased and E2F ex-
150 pression decreased, in response to ATRA exposure (Fig. 5A). We then used the ratio of
151 these values in a polynomial model to calculate the fraction of HL-60 cells in G0 arrest
152 following the addition of ATRA (Fig. 5B). The third-order polynomial model captured the
153 trend in measured G0-arrest values as a function of time, and was robust to uncertainty
154 in the measured data (Fig. 5B, gray). Taken together, the output of the signal integra-
155 tion and phenotypic modules was consistent with time-series and steady-state measure-
156 ments, thereby validating the assumed molecular connectivity. Moreover, outputs from
157 the phenotype module described the trend in ATRA-induced G0 cell cycle arrest. Next,
158 we explored which nodes and interactions between nodes in the signal integration module
159 most influenced the system response.

160 The PU.1 and AP1 proteins were important regulators of ATRA-induced signal inte-
161 gration and phenotypic change (Fig. 6). We conducted pairwise knock simulations of
162 genes in the signal integration and phenotype modules to estimate which nodes con-
163 trolled the processing of the Trigger and cRaF-S621 signals. The difference between the
164 system state with and without the gene knockouts (encoded as a state displacement ma-
165 trix) was decomposed using Singular Value Decomposition (SVD). All simulations were
166 conducted using the best fit parameter set. The first four modes described >99% of the
167 gene knockout variance, with the most important components of these modes being the
168 PU.1 and AP1 proteins, and to a much lesser extent Gfi1 and C/EBPa (Fig. 6A). To better
169 understand which connections involving the PU.1 and AP1 proteins were important, we
170 simulated the pairwise deletion of interactions between these proteins and their respective
171 regulatory targets. SVD decomposition of the state displacement matrix assembled from
172 the pairwise deletion of interactions, suggested the first five modes accounted for >99%
173 of the variance resulting from deletion of the interactions. The most sensitive interactions
174 for the PU.1 protein involved the C/EBPa-dependent regulation of P47Phox expression,

and to a lesser extent AP1 and EGR1 expression (Fig. 6B). On the other other, the most sensitive connections for AP1 involved the C/EBPa-dependent regulation of p21 expression, and the mutual activation of PU.1 and AP1 expression. Taken together, these results suggested that the PU.1 and AP1 proteins acted as important self-reinforcing regulators for both the signal integration and phenotype modules. The analysis suggested that the PU.1 signaling axis promoted the formation of the neutrophil NADPH oxidase (through p47Phox), while AP1 was responsible for cell cycle arrest (through p21). However, this analysis did not give insight into which upstream components of the signal initiation module were important. Toward this question, we explored the composition and regulation of the signalsome complex by experimentally interrogating a panel of possible Raf interaction partners.

The composition of the signalsome, and the kinase ultimately responsible for mediating ATRA-induced Raf activation is currently unknown. To explore this question, we conducted immunoprecipitation and subsequent Western blotting to identify physical interactions between Raf and 19 putative interaction partners. A panel of 19 possible Raf interaction partners (kinases, GTPases, scaffolding proteins etc) was constructed based upon known signaling pathways. We did not consider the most likely binding partner, the small GTPase RAS, as previous studies have ruled it out in MAPK activation in HL-60 cells (20, 27). Total Raf was used as a bait protein for the immunoprecipitation studies. Interrogation of the Raf interactome suggested Vav1 was involved with ATRA-induced initiation of MAPK activity (Fig. 7). Western blot analysis using total Raf and pS621 Raf specific antibodies confirmed the presence of the bait protein, total and phosphorylated forms, in the immunoprecipitate (Fig. 7A). Of the 19 proteins sampled, Vav1, Src, CK2, Akt, and 14-3-3 precipitated with Raf, suggesting a direct physical interaction was possible. However, only the associations between Raf and Vav1 and Raf and Src were ATRA-inducible (Fig. 7). Furthermore, the Vav1 and Src associations were correlated with pS621 Raf

abundance in the precipitate. Others proteins e.g., CK2, Akt and 14-3-3, generally bound Raf regardless of phosphorylation status or ATRA treatment. The remaining 14 proteins were expressed in whole cell lysate (Fig. 7B), but were not detectable in the precipitate of Raf IP. Treatment with the Raf kinase inhibitor GW5074 following ATRA exposure reduced the association of both Vav1 with Raf and Src with Raf (Fig. 7), although the signal intensity for Src was notably weak. However, GW5074 did not influence the association of CK2 or 14-3-3 with Raf, further demonstrating their independence from Raf phosphorylation. Interestingly, the Raf-Akt interaction qualitatively increased following treatment with GW5074; however, it remained unaffected by treatment with ATRA. Src family kinases are known to be important in myeloid differentiation (28) and their role in HL-60 differentiation has been investigated elsewhere (11). Given the existing work and variable reproducibility in the context of the Raf immunoprecipitate, we did not investigate the role of Src further in this study. Taken together, the immunoprecipitation and GW5074 results implicated Vav1 association to be correlated with Raf activation following ATRA-treatment. Previous studies demonstrated that a Vav1-Slp76-Cbl-CD38 complex plays an important role in ATRA-induced MAPK activation and differentiation of HL-60 cells (13). Here we did not observe direct interaction of Raf with Cbl or Slp76; however, this complex could be involved upstream. Next, we considered the effect of the Raf kinase inhibitor GW5074 on functional markers of ATRA-induced growth arrest and differentiation.

Inhibition of Raf kinase activity modulated MAPK activation and differentiation markers following ATRA exposure (Fig. 7D-F). ATRA treatment alone statistically significantly increased the G1/G0 percentage over the untreated control, while GW5074 alone had a negligible effect on the cell cycle distribution (Fig. 7D). Surprisingly, the combination of GW5074 and ATRA statistically significantly increased the G1/G0 population ($82 \pm 1\%$) compared with ATRA alone ($61 \pm 0.5\%$). Increased G1/G0 arrest following the combined treatment with GW5074 and ATRA was unexpected, as the combination of ATRA and the

227 MEK inhibitor (PD98059) has been shown previously to decrease ATRA-induced growth
228 arrest (8). However, growth arrest is not the sole indication of functional differentiation.
229 Expression of the cell surface marker CD11b has also been shown to coincide with HL-60
230 cells myeloid differentiation (29). We measured CD11b expression, for the various treat-
231 ment groups, using immuno-fluorescence flow cytometry 48 hr post-treatment. As with
232 G1/G0 arrest, ATRA alone increased CD11b expression over the untreated control, while
233 GW5074 further enhanced ATRA-induced CD11b expression (Fig. 7E). GW5074 alone
234 had no statistically significant effect on CD11b expression, compared with the untreated
235 control. Lastly, the inducible reactive oxygen species (ROS) response was used as a func-
236 tional marker of differentiated neutrophils (16). We measured the ROS response induced
237 by the phorbol ester 12-O-tetradecanoylphorbol-13-acetate (TPA) using flow cytometry.
238 Untreated cells showed no discernible TPA response, with only $7.0 \pm 3.0\%$ ROS induction
239 (Fig. 7F). Cells treated with ATRA had a significantly increased TPA response, $53 \pm 7\%$
240 ROS induction 48 hr post-treatment. Treatment with both ATRA and GW5074 statistically
241 significantly reduced ROS induction ($22 \pm 0.6\%$) compared to ATRA alone. Interestingly,
242 Western blot analysis did not detect a GW5074 effect on ATRA-induced expression of
243 p47phox, a required upstream component of the ROS response (Fig. 7F, bottom). Thus,
244 the inhibitory effect of GW5074 on inducible ROS might occur downstream of p47phox
245 expression. However, the ROS producing complex is MAPK dependent, therefore it is
246 also possible that GW5074 inhibited ROS production by interfering with MAPK activation
247 (in which case the p47Phox marker might not accurately reflect phenotypic conversion
248 and differentiation).

249 **Discussion**

250 In this study, we presented an effective model of ATRA-inducible differentiation of HL-60
251 cells. The model consisted of three modules: a signal initiation module that sensed and
252 transformed the ATRA signal into activated cRaf-pS621 and the ATRA-RXR/RAR (Trig-
253 ger) signals; a signal integration module that controlled the expression of upstream tran-
254 scription factors given cRaf-pS621 and activated Trigger signals; and a phenotype mod-
255 ule which encoded the expression of functional differentiation markers from the ATRA-
256 inducible transcription factors. The model described the transcription and translation of
257 genes in each module, and signaling events in each module in a growing population of
258 HL-60 cells. Model parameters were largely taken from literature, however, unknown
259 coefficients were estimated from protein measurements in HL-60 cells following ATRA
260 exposure. Despite its simplicity, the effective model captured key features of the ATRA
261 induced differentiation such as sustained MAPK activation, and bistability with respect
262 to ATRA exposure. The model also described the expression of upstream transcription
263 factors which regulated the expression of differentiation markers. Lastly, analysis of the
264 response of the model to perturbations identified PU.1 and AP1 as master regulators of
265 ATRA-induced differentiation. We also reported a new ATRA-inducible component of the
266 signalsome, Vav1. Vav1 is a guanine nucleotide exchange factor for Rho family GTPases
267 that activate pathways leading to actin cytoskeletal rearrangements and transcriptional al-
268 terations (30). The Vav1/Raf association correlated with Raf activity, was ATRA-inducible
269 and decreased after treatment with the Raf inhibitor GW5074.

270 Man-made engineered systems, or naturally occurring cell fate decision programs in-
271 corporate reinforcing feedback and bistability (31, 32). One of the most well studied cell
272 fate circuits is the Mos mitogen-activated protein kinase cascade in *Xenopus* oocytes.
273 This cascade is activated when oocytes are induced by the steroid hormone proges-
274 terone (33). The MEK-dependent activation of p42 MAPK stimulates the accumulation

275 of the Mos oncoprotein, which in turn activates MEK, thereby closing the feedback loop.
276 This is similar to the signal initiation module presented here; ATRA drives signalsome for-
277 mation, which activates MAPK, which in turn leads to more signalsome activation. Thus,
278 while HL-60 and *Xenopus* oocytes are vastly different biological models, their cell fate
279 programs share a similar architectural feature. Reinforcing feedback and bistability has
280 also been implicated in hematopoietic cell fate determination. Laslo et al showed that
281 the counter antagonistic repressors, Gfi-1 and Egr-1/2 (whose expression is tuned by
282 PU.1 and C/EBPa), encodes a bistable switch that results in a macrophage, neutrophil
283 or a mixed lineage population depending upon PU.1 and C/EBPa expression (32). The
284 current model contained the Gfi-1 and Egr-1/2 agonistic switch; however, its significance
285 was unclear for HL-60 cells. Other unrelated cell fate decisions such as programmed cell
286 death have also been suggested to be bistable (34). Still more biochemical networks im-
287 portant to human health, for example the human coagulation or complement cascades,
288 also feature strong positive feedback elements (35). Thus, while reinforcing feedback is
289 often undesirable in human engineered systems, it is at the core of a diverse variety of
290 cell fate programs and other networks important to human health.

291 Analysis of the signal integration and phenotype modules suggested that PU.1 and
292 AP1 regulated distinct phenotypic axes following ATRA exposure. The PU.1 transcription
293 factor, a member of the ets transcription factor family, is a well known regulatory protein
294 in granulocyte and monocyte development (36). The relative level of PU.1 and C/EBPa
295 regulates macrophage versus neutrophil cell fate decisions in granulocytic macrophage
296 progenitor cells (37).

297 Immunoprecipitation studies identified a limited number of ATRA-dependent and -
298 independent Raf interaction partners. While we were unable to detect the association
299 of Raf with common kinases and GTPases such as PKC, PKA, p38, Rac and Rho, we
300 did establish potential interactions between Raf and key partners such as Vav1, Src, Akt,

301 CK2 and 14-3-3. All of these partners are known to be associated with Raf activation
302 or function. Src is known to bind Raf through an SH2 domain, and this association has
303 been shown to be dependent of the serine phosphorylation of Raf (38). Thus, an ATRA in-
304 ductible Src/Raf association may be a result of ATRA-induced Raf phosphorylation at S259
305 or S621. We also identified an interaction between Raf and the Ser/Thr kinases Akt and
306 CK2. Akt can phosphorylate Raf at S259, as demonstrated by studies in a human breast
307 cancer line (39). CK2 can also phosphorylate Raf, although the literature has traditionally
308 focused on S338 and not S621 or S259(40). However, neither of these kinase interactions
309 were ATRA-inducible, suggesting their association with Raf alone was not associated with
310 ATRA-induced Raf phosphorylation. The adapter protein 14-3-3 was also constitutively
311 associated with Raf. The interaction between Raf and 14-3-3 has been associated with
312 both S621 and S259 phosphorylation and activity (41). Additionally, the association of
313 Raf with 14-3-3 not only stabilized S621 phosphorylation, but also reversed the S621
314 phosphorylation from inhibitory to activating (42). Finally, we found that Vav1/Raf associ-
315 ation correlated with Raf activity, was ATRA-inducible and decreased after treatment with
316 GW5074. The presence of Vav1 in Raf/Grb2 complexes has been shown to correlate with
317 increased Raf activity in mast cells (43). Furthermore, studies on Vav1 knockout mice
318 demonstrated that the loss of Vav1 resulted in deficiencies of ERK signaling for both T-
319 cells as well as neutrophils (44, 45). Interestingly, while an integrin ligand-induced ROS
320 response was blocked in Vav1 knockout neutrophils, TPA was able to bypass the Vav1
321 requirement and stimulate both ERK phosphorylation and ROS induction (45). In this
322 study, the TPA-induced ROS response was dependent upon Raf kinase activity, and was
323 mitigated by the addition of GW5074. It is possible that Vav1 is downstream of various
324 integrin receptors but upstream of Raf in terms of inducible ROS responses. Vav1 has
325 also been shown to associate with a Cbl-Slp76-CD38 complex in an ATRA-dependent
326 manner; furthermore, transfection of HL-60 cells with Cbl mutants that fail to bind CD38,

327 yet still bind Slp76 and Vav1, prevents ATRA-induced MAPK activation (13). The literature
328 suggest a variety of possible receptor-signaling pathways, which involve Vav1, for MAPK
329 activation; moreover, given the ATRA-inducible association Vav1 may play a direct role in
330 Raf activation.

331 We hypothesized that Vav1 is a member of an ATRA-inducible complex which propels
332 sustained MAPK activation, arrest and differentiation. Initially, ATRA-induced Vav1 ex-
333 pression drives increased association between Vav1 and Raf. This increased interaction
334 facilitates phosphorylation and activation of Raf by pre-bound Akt and/or CK2 at S621
335 or perhaps S259. Constitutively bound 14-3-3 may also stabilize the S621 phosphory-
336 lation, modulate the activity and/or up-regulate autophosphorylation. Activated Raf can
337 then drive ERK activation, which in turn closes the positive feedback loop by activating
338 Raf transcription factors e.g., Sp1 and/or STAT1 (46–49). We tested this working hy-
339 pothesis using mathematical modeling. The model recapitulated both ATRA time-course
340 data as well as the GW5074 inhibitor effects. This suggested the proposed Raf-Vav1
341 architecture was at least consistent with the experimental studies. Further, analysis of
342 the Raf-Vav1 model identified bistability in ppERK levels. Thus, two possible MAPK ac-
343 tivation branches were possible for experimentally testable ATRA values. The analysis
344 also suggested the ATRA-induced Raf-Vav1 architecture could be locked into a sustained
345 signaling mode (high ppERK) even in the absence of a ATRA signal. This locked-in prop-
346 erty could give rise to an ATRA-induction memory. We validated the treatment memory
347 property predicted by the Raf-Vav1 circuit experimentally using ATRA-washout experi-
348 ments. ERK phosphorylation levels remained high for more then 96 hr after ATRA was
349 removed. Previous studies demonstrated that HL-60 cells possessed an inheritable mem-
350 ory of ATRA stimulus (50). Although the active state was self-sustaining, the inactive state
351 demonstrated considerable robustness to perturbation. For example, we found that 50x
352 overexpression of Raf was required to reliably lock MAPK into the activated state, while

353 small perturbations had almost no effect on ppERK levels over the entire ensemble. CD38
354 expression correlated with the ppERK, suggesting its involvement in the signaling com-
355 plex. Our computational and experimental results showed that positive feedback, through
356 ERK-dependent Raf expression, could sustain MAPK signaling through many division cy-
357 cles. Such molecular mechanisms could underly aspects of cellular memory associated
358 to consecutive ATRA treatments.

359 There were several issues that can be explored further with the effective ATRA differ-
360 entiation model. First, there was likely missing connectivity in the effective differentiation
361 circuit. Decreasing BLR1 expression with simultaneously sustained cRaf-pS261 activa-
362 tion was not captured by the current network architecture. This suggested that signal-
363 some, once activated, had a long lifetime as decreased BLR1 expression did not impact
364 cRaf-pS261 abundance. We could model this by separating signalsome formation into an
365 inactive precursor pool that is transformed to a long-lived activated signalsome by MAPK
366 activation. We should also explore adding additional downstream biological modules to
367 this skeleton model, for example the upregulation of reactive oxygen markers such as
368 p47Phox or cell cycle arrest components to capture the switch from an actively prolifer-
369 ating population to a population in G0-arrest. Next, the choice of max/min integration
370 rules or the particular form of the transfer functions could also be explored. Integration
371 rules other than max/min could be used, such as the mean or the product, assuming the
372 range of the transfer functions is always $f \in [0, 1]$. Alternative integration rules might
373 have different properties which could influence model identification or performance. For
374 example, a mean integration rule would be differentiable, allowing derivative-based opti-
375 mization approaches to be used. The form of the transfer function could also be explored.
376 We choose hill-like functions because of their prominence in the systems and synthetic
377 biology community. However, many other transfer functions are possible.

378 **Materials and Methods**

379 *Effective gene expression model equations.* We decomposed the ATRA-induced differ-
 380 entiation program into three modules; a signal initiation module that sensed and trans-
 381 formed the ATRA signal into activated cRaf-pS621 and the ATRA-RXR/RAR (activated
 382 Trigger) signals; a signal integration module that controlled the expression of upstream
 383 transcription factors given cRaf-pS621 and activated Trigger signals; and a phenotype
 384 module which encoded the expression of functional differentiation markers from the ATRA-
 385 inducible transcription factors. The output of the signal initiation module was the input to
 386 the gene expression model. For each gene $j = 1, 2, \dots, \mathcal{G}$, we modeled both the mRNA
 387 (m_j), protein (p_j) and signaling species abundance:

$$\frac{dm_j}{dt} = r_{T,j} - (\mu + \theta_{m,j}) m_j + \lambda_j \quad (1)$$

$$\frac{dp_j}{dt} = r_{X,j} - (\mu + \theta_{p,j}) p_j \quad (2)$$

$$g(p_1, \dots, p_{\mathcal{G}}, \kappa) = 0 \quad (3)$$

388 The terms $r_{T,j}$ and $r_{X,j}$ denote the specific rates of transcription, and translation while
 389 the terms $\theta_{m,j}$ and $\theta_{p,j}$ denote first-order degradation constants for mRNA and protein,
 390 respectively. The specific transcription rate $r_{T,j}$ was modeled as the product of a kinetic
 391 term $\bar{r}_{T,j}$ and a control term u_j which described how the abundance of transcription fac-
 392 tors, or other regulators influenced the expression of gene j . The kinetic transcription
 393 term $\bar{r}_{T,j}$ was modeled as:

$$\bar{r}_{T,j} = V_T^{max} \left(\frac{L_{T,o}}{L_{T,j}} \right) \left(\frac{G_j}{K_T + G_j} \right) \quad (4)$$

394 where the maximum gene expression rate V_T^{max} was defined as the product of a char-
 395 acteristic transcription rate constant (k_T) and the abundance of RNA polymerase (R_1),

396 $V_T^{max} = k_T(R_1)$. The $(L_{T,o}/L_{T,j})$ term denotes the ratio of transcription read lengths; $L_{T,o}$
 397 represents a characteristic gene length, while $L_{T,j}$ denotes the length of gene j . Thus,
 398 the ratio $(L_{T,o}/L_{T,j})$ is a gene specific correction to the characteristic transcription rate
 399 V_T^{max} . The degradation rate constants were defined as $\theta_{m,j}$ and $\theta_{p,j}$ denote characteristic
 400 degradation constants for mRNA and protein, respectively. Lastly, the λ_j term denotes the
 401 constitutive rate of expression of gene j .

402 The gene expression control term $0 \leq u_j \leq 1$ depended upon the combination of fac-
 403 tors which influenced the expression of gene j . If the expression of gene j was influenced
 404 by $1, \dots, m$ factors, we modeled this relationship as $u_j = \mathcal{I}_j(f_{1j}(\cdot), \dots, f_{mj}(\cdot))$ where
 405 $0 \leq f_{ij}(\cdot) \leq 1$ denotes a regulatory transfer function quantifying the influence of factor i
 406 on the expression of gene j , and $\mathcal{I}_j(\cdot)$ denotes an integration rule which combines the
 407 individual regulatory inputs for gene j into a single control term. In this study, the integra-
 408 tion rule governing gene expression was the weighted fraction of promoter configurations
 409 that resulted in gene expression (51):

$$u_j = \frac{W_{R_{1,j}} + \sum_n W_{nj} f_{nj}}{1 + W_{R_{1,j}} + \sum_d W_{dj} f_{dj}} \quad (5)$$

410 The numerator, the weighted sum (with weights W_{nj}) of promoter configurations leading to
 411 gene expression, was normalized by all possible promoter configurations. The likelihood
 412 of each configuration was quantified by the transfer function f_{nj} (which we modeled using
 413 hill like functions), while the lead term in the numerator $W_{R_{1,j}}$ denotes the weight of con-
 414 stitutive expression for gene j . Given this formulation, the rate of constitutive expression
 415 was then given by:

$$\lambda_j = \bar{r}_{T,j} \left(\frac{W_{R_{1,j}}}{1 + W_{R_{1,j}}} \right) \quad (6)$$

416 If a gene expression process had no modifying factors, $u_j = 1$. Lastly, the specific trans-

417 lation rate was modeled as:

$$r_{X,j} = V_X^{\max} \left(\frac{L_{X,o}}{L_{X,j}} \right) \left(\frac{m_j}{K_X + m_j} \right) \quad (7)$$

418 where V_X^{\max} denotes a characteristic maximum translation rate estimated from literature,
419 and K_X denotes a translation saturation constant. The characteristic maximum translation
420 rate was defined as the product of a characteristic translation rate constant (k_X) and
421 the Ribosome abundance (R_2), $V_X^{\max} = k_X (R_2)$. As was the case for transcription, we
422 corrected the characteristic translation rate by the ratio of the length of a characteristic
423 transcription normalized by the length of transcript j .

424 *Signaling model equations.* The signal initiation, and integration modules required the
425 abundance of cRaf-pS621 and ATRA-RXR/RAR (activated Trigger) as inputs. However,
426 our base model described only the abundance of inactive proteins e.g., cRaf or RXR/RAR
427 but not the activated forms. To address this issue, we estimated pseudo steady state
428 approximations for the abundance of cRaf-pS621 and activated Trigger (shown generally
429 as Eq (3)). The abundance of activated trigger ($x_{a,1}$) was estimated directly from the
430 RXR/RAR abundance ($x_{u,1}$):

$$x_{a,1} \sim x_{u,1} \left(\frac{\alpha \cdot \text{ATRA}}{1 + \alpha \cdot \text{ATRA}} \right) \quad (8)$$

431 where α denotes a gain parameter; $\alpha = 0.0$ if ATRA is less than a threshold, and $\alpha = 0.1$
432 if ATRA is greater than the differentiation threshold. The abundance of cRaf-pS621 was
433 estimated by making the pseudo steady state approximation on the cRaf-pS621 balance.
434 The abundance of an activated signaling species i was given by:

$$\frac{dx_i}{dt} = r_{+,i}(\mathbf{x}, \mathbf{k}) - (\mu + k_{d,i}) x_i \quad i = 1, \dots, \mathcal{M} \quad (9)$$

435 The quantity x_i denotes concentration of signaling species i , while \mathcal{R} and \mathcal{M} denote
 436 the number of signaling reactions and signaling species in the model, respectively. The
 437 term $r_{+,i}(\mathbf{x}, \mathbf{k})$ denotes the rate of generation of activated species i , while μ denotes
 438 the specific growth rate, and $k_{d,i}$ denotes the rate constant controlling the non-specific
 439 degradation of x_i . We neglected deactivation reactions e.g., phosphatase activities. We
 440 assumed that signaling processes were fast compared to gene expression; this allowed
 441 us to approximate the signaling balance as:

$$x_i^* \simeq \frac{r_{+,i}(\mathbf{x}, \mathbf{k})}{(\mu + k_{d,i})} \quad i = 1, \dots, \mathcal{M} \quad (10)$$

442 The generation rate was written as the product of a kinetic term ($\bar{r}_{+,i}$) and a control term
 443 (v_i). The control terms $0 \leq v_j \leq 1$ depended upon the combination of factors which in-
 444 fluenced rate process j . If rate j was influenced by $1, \dots, m$ factors, we modeled this
 445 relationship as $v_j = \mathcal{I}_j(f_{1j}(\cdot), \dots, f_{mj}(\cdot))$ where $0 \leq f_{ij}(\cdot) \leq 1$ denotes a regulatory
 446 transfer function quantifying the influence of factor i on rate j . The function $\mathcal{I}_j(\cdot)$ is an
 447 integration rule which maps the output of regulatory transfer functions into a control vari-
 448 able. In this study, we used $\mathcal{I}_j \in \{\min, \max\}$ and hill transfer functions (52). If a process
 449 had no modifying factors, $v_j = 1$. The kinetic rate of cRaf-pS621 generation $\bar{r}_{+,cRaf}$ was
 450 modeled as:

$$\bar{r}_{+,cRaf} = k_{+,cRaf} x_s \left(\frac{x_{cRaf}}{K_{+,cRaf} + x_{cRaf}} \right) \quad (11)$$

451 where x_s denotes the signalsome abundance, and $K_{+,cRaf}$ denotes a saturation constant
 452 governing cRaf-pS621 formation. The formation of cRaf-pS621 was regulated by only a
 453 single factor, the abundance of MAPK inhibitor, thus $v_{+,cRaf}$ took the form:

$$v_{+,cRaf} = \left(1 - \frac{I}{K_D + I} \right) \quad (12)$$

454 where I denotes the abundance of the MAPK inhibitor, and K_D denotes the inhibitor
455 affinity.

456 *Estimation of gene expression model parameters.* We estimated parameters appearing
457 in the mRNA and protein balances, the abundance of polymerases and ribosomes, tran-
458 scription and translation rates, the half-life of a typical mRNA and protein, and typical
459 values for the copies per cell of RNA polymerase and ribosomes from literature (Table 2).
460 The saturation constants K_X and K_T were adjusted so that gene expression and trans-
461 lation resulted in gene products on a biologically realistic concentration scale. Lastly, we
462 calculated the concentration for gene G_j by assuming, on average, that a cell had two
463 copies of each gene at any given time. Thus, the bulk of our gene expression model pa-
464 rameters were based directly upon literature values, and were not adjusted during model
465 identification. However, the remaining parameters, e.g., the W_{ij} appearing in the gene
466 expression control laws, or parameters appearing in the transfer functions f_{dij} , were esti-
467 mated from the protein expression and signaling data sets discussed here.

468 Signaling and gene expression model parameters were estimated by minimizing the
469 squared difference between simulations and experimental protein data set j . We mea-
470 sured the squared difference in the scale, fold change and shape for protein j :

$$E_j(\mathbf{k}) = \left(\mathcal{M}_j(t_-) - \hat{y}_j(t_-, \mathbf{k}) \right)^2 + \sum_{i=1}^{\mathcal{T}_j} \left(\hat{\mathcal{M}}_{ij} - \hat{y}_{ij}(\mathbf{k}) \right)^2 + \sum_{i=1}^{\mathcal{T}_j} \left(\mathcal{M}'_{ij} - y'_{ij}(\mathbf{k}) \right)^2 \quad (13)$$

471 The first term in Eqn. (13) quantified the initial *scale* error, directly before the addition
472 of ATRA. In this case, $\mathcal{M}_j(t_-)$ (the approximate concentration of protein j before the
473 addition of ATRA) was estimated from literature. This term was required because the
474 protein measurements were reported as the fold-change; thus, the data was normalized
475 by a control value measured before the addition of ATRA. However, the model operated on
476 a physical scale. The first term allowed the model to capture physically realistic changes

477 following ATRA addition. The second term quantified the difference in the *fold-change* of
 478 protein j as a function of time. The terms $\hat{\mathcal{M}}_{ij}$ and \hat{y}_{ij} denote the scaled experimental
 479 observations and simulation outputs (fold-change; protein normalized by control value
 480 directly before ATRA addition) at time i from protein j , where T_j denoted the number of
 481 time points for data set j . Lastly, the third term of the objective function measured the
 482 difference in the *shape* of the measured and simulated protein levels. The scaled value
 483 $0 \leq \mathcal{M}'_{ij} \leq 1$ was given by:

$$\hat{\mathcal{M}}_{ij} = \left(\mathcal{M}_{ij} - \min_i \mathcal{M}_{ij} \right) / \left(\max_i \mathcal{M}_{ij} - \min_i \mathcal{M}_{ij} \right) \quad (14)$$

484 where $\mathcal{M}'_{ij} = 0$ and $\mathcal{M}'_{ij} = 1$ describe the lowest (highest) intensity bands. A similar
 485 scaling was used for the simulation output. We minimized the total model residual $\sum_j E_j$
 486 using a heuristic direct-search optimization procedure, subject to box constraints on the
 487 parameter values, starting from a random initial parameter guess. Each downhill step was
 488 archived and used for ensemble calculations. The optimization procedure (a covariance
 489 matrix adaptation evolution strategy) has been reported previously (53).

490 *Estimation of an effective cell cycle arrest model.* We formulated an effective N-order
 491 polynomial model of the fraction of cells undergoing ATRA-induced cell cycle arrest at
 492 time t , $\hat{\mathcal{A}}(t)$, as:

$$\hat{\mathcal{A}}(t) \simeq a_0 + \sum_{i=1}^{N-1} a_i \phi_i(\mathbf{p}(t), t) \quad (15)$$

493 where a_i were unknown parameters, and $\phi_i(\mathbf{p}(t), t)$ denotes a basis function. The basis
 494 functions were dependent upon the system state; in this study, we assumed $N = 4$ and
 495 basis functions of the form:

$$\phi_i(\mathbf{p}(t), t) = \left(\frac{t}{T} + \frac{p21}{E2F} \Big|_t \right)^{(i-1)} \quad (16)$$

496 The parameters a_0, \dots, a_3 were estimated directly from cell-cycle measurements (biologi-
497 cal replicates) using least-squares.

498 *Availability of model code.* The signaling and gene expression model equations, and the
499 parameter estimation procedure, were implemented in the Julia programming language.
500 The model equations were solved using the ODE23s routine of the ODE package (54). The
501 model code and parameter ensemble is freely available under an MIT software license
502 and can be downloaded from <http://www.varnerlab.org>.

503 *Cell culture and treatment* Human myeloblastic leukemia cells (HL-60 cells) were grown
504 in a humidified atmosphere of 5% CO₂ at 37°C and maintained in RPMI 1640 from Gibco
505 (Carlsbad, CA) supplemented with 5% heat inactivated fetal bovine serum from Hyclone
506 (Logan, UT) and 1× antibiotic/antimicotic (Gibco, Carlsbad, CA). Cells were cultured in
507 constant exponential growth (55). Experimental cultures were initiated at 0.1×10^6 cells/mL
508 24 hr prior to ATRA treatment; if indicated, cells were also treated with GW5074 (2 μ M) 18
509 hr before ATRA treatment. For the cell culture washout experiments, cells were treated
510 with ATRA for 24 hr, washed 3x with prewarmed serum supplemented culture medium
511 to remove ATRA, and reseeded in ATRA-free media as described. Western blot analysis
512 was performed at incremental time points after removal of ATRA.

513 *Chemicals* All-Trans Retinoic Acid (ATRA) from Sigma-Aldrich (St. Louis, MO) was dis-
514 solved in 100% ethanol with a stock concentration of 5mM, and used at a final concen-
515 tration of 1 μ M (unless otherwise noted). The cRaf inhibitor GW5074 from Sigma-Aldrich
516 (St. Louis, MO) was dissolved in DMSO with a stock concentration of 10mM, and used
517 at a final concentration of 2 μ M. HL-60 cells were treated with 2 μ M GW5074 with or with-
518 out ATRA (1 μ M) at 0 hr. This GW5074 dosage had a negligible effect on the cell cycle
519 distribution, compared to ATRA treatment alone.

520 *Immunoprecipitation and western blotting* Approximately 1.2×10^7 cells were lysed using
521 $400\mu\text{L}$ of M-Per lysis buffer from Thermo Scientific (Waltham, MA). Lysates were cleared
522 by centrifugation at $16,950 \times g$ in a micro-centrifuge for 20 min at 4°C . Lysates were
523 pre-cleared using $100\mu\text{L}$ protein A/G Plus agarose beads from Santa Cruz Biotechnology
524 (Santa Cruz, CA) by inverting overnight at 4°C . Beads were cleared by centrifugation and
525 total protein concentration was determined by a BCA assay (Thermo Scientific, Waltham,
526 MA). Immunoprecipitations were setup by bringing lysate to a concentration of 1g/L in a
527 total volume of $300\mu\text{L}$ (M-Per buffer was used for dilution). The anti-Raf antibody was
528 added at $3\mu\text{L}$. A negative control with no bait protein was also used to exclude the di-
529 rect interaction of proteins with the A/G beads. After 1 hr of inversion at 4°C , $20\mu\text{L}$ of
530 agarose beads was added and samples were left to invert overnight at 4°C . Samples
531 were then washed three times with M-Per buffer by centrifugation. Finally proteins were
532 eluted from agarose beads using a laemmli loading buffer. Eluted proteins were resolved
533 by SDS-PAGE and Western blotting. Total lysate samples were normalized by total protein
534 concentration ($20\mu\text{g}$ per sample) and resolved by SDS-PAGE and Western blotting. Sec-
535 ondary HRP bound antibody was used for visualization. All antibodies were purchased
536 from Cell Signaling (Boston, MA) with the exception of α -p621 Raf which was purchased
537 from Biosource/Invitrogen (Carlsbad, CA), and α -CK2 from BD Biosciences (San Jose,
538 CA).

539 *Morphology assessment* Untreated and ATRA-treated HL-60 cells were collected after
540 72 hr and cytocentrifuged for 3 min at 700 rpm onto glass slides. Slides were air-dried
541 and stained with Wright's stain. Slide images were captured at 40X (Leica DM LB 100T
542 microscope, Leica Microsystems).

543 **Competing interests**

544 The authors declare that they have no competing interests.

545 **Author's contributions**

546 J.V and A.Y directed the study. R.T, H.J, R.B and J.C conducted the cell culture measure-
547 ments. J.V, R.B, W.D, K.R and A.S developed the reduced order HL-60 models and the
548 parameter ensemble. W.D and J.V analyzed the model ensemble, and generated figures
549 for the manuscript. The manuscript was prepared and edited for publication by W.D, A.Y
550 and J.V.

551 **Acknowledgements**

552 We gratefully acknowledge the suggestions from the anonymous reviewers to improve
553 this manuscript.

554 **Funding**

555 We acknowledge the financial support to J.V. by the National Science Foundation CA-
556 REER (CBET-0846876) for the support of R.T. and H.J. In addition, we acknowledge
557 support to A.Y. from the National Institutes of Health (CA 30555, CA152870) and a grant
558 from New York State Stem Cell Science. Lastly, we acknowledge the financial support to
559 J.V. and A.Y. from the National Cancer Institute (#U54 CA143876). The content is solely
560 the responsibility of the authors and does not necessarily represent the official views of
561 the National Cancer Institute or the National Institutes of Health.

562 **References**

- 563 1. Bushue N, Wan YJY (2010) Retinoid pathway and cancer therapeutics. *Adv Drug
564 Deliv Rev* 62: 1285-98.
- 565 2. Tang XH, Gudas LJ (2011) Retinoids, retinoic acid receptors, and cancer. *Annu Rev
566 Pathol* 6: 345-64.
- 567 3. Cheung FSG, Lovicu FJ, Reichardt JKV (2012) Current progress in using vitamin d
568 and its analogs for cancer prevention and treatment. *Expert Rev Anticancer Ther*
569 12: 811-37.
- 570 4. Nilsson B (1984) Probable in vivo induction of differentiation by retinoic acid of
571 promyelocytes in acute promyelocytic leukaemia. *Br J Haematol* 57: 365-71.
- 572 5. Warrell RP Jr (1993) Retinoid resistance in acute promyelocytic leukemia: new
573 mechanisms, strategies, and implications. *Blood* 82: 1949-53.
- 574 6. Freemantle SJ, Spinella MJ, Dmitrovsky E (2003) Retinoids in cancer therapy and
575 chemoprevention: promise meets resistance. *Oncogene* 22: 7305-15.
- 576 7. Breitman TR, Selonick SE, Collins SJ (1980) Induction of differentiation of the hu-
577 man promyelocytic leukemia cell line (HL-60) by retinoic acid. *Proc Natl Acad Sci U
578 S A* 77: 2936–2940.
- 579 8. Yen A, Roberson MS, Varvayanis S, Lee AT (1998) Retinoic acid induced
580 mitogen-activated protein (MAP)/extracellular signal-regulated kinase (ERK) kinase-
581 dependent MAP kinase activation needed to elicit HL-60 cell differentiation and
582 growth arrest. *Cancer Res* 58: 3163–3172.
- 583 9. Hong HY, Varvayanis S, Yen A (2001) Retinoic acid causes MEK-dependent RAF
584 phosphorylation through RARalpha plus RXR activation in HL-60 cells. *Differentia-
585 tion* 68: 55–66.
- 586 10. Mangelsdorf DJ, Ong ES, Dyck JA, Evans RM (1990) Nuclear receptor that identifies
587 a novel retinoic acid response pathway. *Nature* 345: 224–229.

- 588 11. Congleton J, MacDonald R, Yen A (2012) Src inhibitors, PP2 and dasatinib, increase
589 retinoic acid-induced association of Lyn and c-Raf (S259) and enhance MAPK-
590 dependent differentiation of myeloid leukemia cells. Leukemia 26: 1180-8.
- 591 12. Shen M, Bunaci R, Congleton J, Jensen H, Sayam L, et al. (2011) Interferon regu-
592 latory factor-1 binds c-Cbl, enhances mitogen activated protein kinase signaling and
593 promotes retinoic acid-induced differentiation of HL-60 human myelo-monoblastic
594 leukemia cells. Leuk Lymphoma 52: 2372-9.
- 595 13. Shen M, Yen A (2009) c-Cbl tyrosine kinase-binding domain mutant G306E abol-
596 ishes the interaction of c-Cbl with CD38 and fails to promote retinoic acid-induced
597 cell differentiation and G0 arrest. J Biol Chem 284: 25664–25677.
- 598 14. Yen A, Varvayanis S, Smith J, Lamkin T (2006) Retinoic acid induces expression of
599 SLP-76: expression with c-FMS enhances ERK activation and retinoic acid-induced
600 differentiation/G0 arrest of HL-60 cells. Eur J Cell Biol 85: 117–132.
- 601 15. Marchisio M, Bertagnolo V, Colamussi ML, Capitani S, Neri LM (1998) Phos-
602 phatidylinositol 3-kinase in HL-60 nuclei is bound to the nuclear matrix and increases
603 during granulocytic differentiation. Biochem Biophys Res Commun 253: 346-51.
- 604 16. Congleton J, Jiang H, Malavasi F, Lin H, Yen A (2011) ATRA-induced HL-60 myeloid
605 leukemia cell differentiation depends on the CD38 cytosolic tail needed for mem-
606 brane localization, but CD38 enzymatic activity is unnecessary. Exp Cell Res 317:
607 910–919.
- 608 17. Wang J, Yen A (2004) A novel retinoic acid-responsive element regulates retinoic
609 acid induced BLR1 expression. Mol Cell Biol 24: 2423 - 2443.
- 610 18. Yen A (1990) HL-60 cells as a model of growth and differentiation: the significance
611 of variant cells. Hematology Review 4: 5-46.
- 612 19. Yang T, Xiong Q, Enslen H, Davis R, Chow CW (2002) Phosphorylation of NFATc4
613 by p38 mitogen-activated protein kinases. Mol Cell Biol 22: 3892–3904.

- 614 20. Wang J, Yen A (2008) A MAPK-positive Feedback Mechanism for BLR1 Signaling
615 Propels Retinoic Acid-triggered Differentiation and Cell Cycle Arrest. *J Biol Chem*
616 283: 4375–4386.
- 617 21. Tasseff R, Nayak S, Song S, Yen A, Varner J (2011) Modeling and analysis of retinoic
618 acid induced differentiation of uncommitted precursor cells. *Integr Biol* 3: 578 - 591.
- 619 22. Jensen HA, Styskal LE, Tasseff R, Bunaciu RP, Congleton J, et al. (2013) The
620 src-family kinase inhibitor pp2 rescues inducible differentiation events in emergent
621 retinoic acid-resistant myeloblastic leukemia cells. *PLoS One* 8: e58621.
- 622 23. Jensen HA, Bunaciu RP, Ibabao CN, Myers R, Varner JD, et al. (2014) Retinoic acid
623 therapy resistance progresses from unilineage to bilineage in hl-60 leukemic blasts.
624 *PLoS One* 9: e98929.
- 625 24. Jensen HA, Bunaciu RP, Varner JD, Yen A (2015) Gw5074 and pp2 kinase inhibitors
626 implicate nontraditional c-raf and lyn function as drivers of retinoic acid-induced mat-
627 uration. *Cell Signal* 27: 1666-75.
- 628 25. Jensen HA, Yourish HB, Bunaciu RP, Varner JD, Yen A (2015) Induced myelomono-
629 cytic differentiation in leukemia cells is accompanied by noncanonical transcription
630 factor expression. *FEBS Open Bio* 5: 789-800.
- 631 26. Milo R, Jorgensen P, Moran U, Weber G, Springer M (2010) Bionumbers—the
632 database of key numbers in molecular and cell biology. *Nucleic Acids Res* 38: D750-
633 3.
- 634 27. Katagiri K, Hattori S, Nakamura S, Yamamoto T, Yoshida T, et al. (1994) Activation
635 of ras and formation of gap complex during tpa-induced monocytic differentiation of
636 hl-60 cells. *Blood* 84: 1780–1789.
- 637 28. Miranda MB, Johnson DE (2007) Signal transduction pathways that contribute to
638 myeloid differentiation. *Leukemia* 21: 1363–1377.
- 639 29. Hickstein DD, Back AL, Collins SJ (1989) Regulation of expression of the cd11b and

- 640 cd18 subunits of the neutrophil adherence receptor during human myeloid differen-
641 tiation. *J Biol Chem* 264: 21812–21817.
- 642 30. Hornstein I, Alcover A, Katzav S (2004) Vav proteins, masters of the world of cy-
643 toskeleton organization. *Cell Signal* 16: 1-11.
- 644 31. Ferrell J (2002) Self-perpetuating states in signal transduction: positive feedback,
645 double-negative feedback and bistability. *Curr Opin Cell Biol* 14: 140-8.
- 646 32. Laslo P, Spooner CJ, Warmflash A, Lancki DW, Lee HJ, et al. (2006) Multilineage
647 transcriptional priming and determination of alternate hematopoietic cell fates. *Cell*
648 126: 755-66.
- 649 33. Xiong W, Ferrell J (2003) A positive-feedback-based bistable 'memory module' that
650 governs a cell fate decision. *Nature* 426: 460-5.
- 651 34. Bagci EZ, Vodovotz Y, Billiar TR, Ermentrout GB, Bahar I (2006) Bistability in apop-
652 tosis: roles of bax, bcl-2, and mitochondrial permeability transition pores. *Biophys J*
653 90: 1546-59.
- 654 35. Luan D, Zai M, Varner JD (2007) Computationally derived points of fragility of a
655 human cascade are consistent with current therapeutic strategies. *PLoS Comput
656 Biol* 3: e142.
- 657 36. Friedman AD (2007) Transcriptional control of granulocyte and monocyte develop-
658 ment. *Oncogene* 26: 6816-28.
- 659 37. Dahl R, Walsh JC, Lancki D, Laslo P, Iyer SR, et al. (2003) Regulation of macrophage
660 and neutrophil cell fates by the PU.1:C/EBPalpha ratio and granulocyte colony-
661 stimulating factor. *Nat Immunol* 4: 1029-36.
- 662 38. Cleghon V, Morrison DK (1994) Raf-1 interacts with fyn and src in a non-
663 phosphotyrosine-dependent manner. *J Biol Chem* 269: 17749–17755.
- 664 39. Zimmermann S, Moelling K (1999) Phosphorylation and regulation of raf by akt (pro-
665 tein kinase b). *Science* 286: 1741–1744.

- 666 40. Ritt DA, Zhou M, Conrads TP, Veenstra TD, Copeland TD, et al. (2007) Ck2 is a
667 component of the ksr1 scaffold complex that contributes to raf kinase activation.
668 Curr Biol 17: 179–184.
- 669 41. Hekman M, Wiese S, Metz R, Albert S, Troppmair J, et al. (2004) Dynamic changes
670 in c-raf phosphorylation and 14-3-3 protein binding in response to growth factor stim-
671 ulation: differential roles of 14-3-3 protein binding sites. J Biol Chem 279: 14074–
672 14086.
- 673 42. Dhillon AS, Yip YY, Grindlay GJ, Pakay JL, Dangers M, et al. (2009) The c-terminus
674 of raf-1 acts as a 14-3-3-dependent activation switch. Cell Signal 21: 1645–1651.
- 675 43. Song JS, Gomez J, Stancato LF, Rivera J (1996) Association of a p95 vav-containing
676 signaling complex with the fcepsiloniori gamma chain in the rbl-2h3 mast cell line.
677 evidence for a constitutive in vivo association of vav with grb2, raf-1, and erk2 in an
678 active complex. J Biol Chem 271: 26962–26970.
- 679 44. Costello PS, Walters AE, Mee PJ, Turner M, Reynolds LF, et al. (1999) The rho-
680 family gtp exchange factor vav is a critical transducer of t cell receptor signals to the
681 calcium, erk, and nf-kappab pathways. Proc Natl Acad Sci U S A 96: 3035–3040.
- 682 45. Graham D, Robertson C, Bautista J, Mascarenhas F, Diacovo M, et al. (2007)
683 Neutrophil-mediated oxidative burst and host defense are controlled by a Vav-
684 PLCgamma2 signaling axis in mice. J Clin Invest 117: 3445–3452.
- 685 46. Kim HS, Lim IK (2009) Phosphorylated extracellular signal-regulated protein kinases
686 1 and 2 phosphorylate sp1 on serine 59 and regulate cellular senescence via tran-
687 scription of p21sdi1/cip1/waf1. J Biol Chem 284: 15475–15486.
- 688 47. Milanini-Mongiat J, Pouyss?gur J, Pag?as G (2002) Identification of two sp1 phos-
689 phorylation sites for p42/p44 mitogen-activated protein kinases: their implication in
690 vascular endothelial growth factor gene transcription. J Biol Chem 277: 20631–
691 20639.

- 692 48. Zhang Y, Cho YY, Petersen BL, Zhu F, Dong Z (2004) Evidence of stat1 phosphory-
693 lation modulated by mapks, mek1 and msk1. *Carcinogenesis* 25: 1165–1175.
- 694 49. Li Z, Theus MH, Wei L (2006) Role of erk 1/2 signaling in neuronal differentiation of
695 cultured embryonic stem cells. *Dev Growth Differ* 48: 513–523.
- 696 50. Yen A, Reece SL, Albright KL (1984) Dependence of hl-60 myeloid cell differentiation
697 on continuous and split retinoic acid exposures: precommitment memory associated
698 with altered nuclear structure. *J Cell Physiol* 118: 277–286.
- 699 51. Moon TS, Lou C, Tamsir A, Stanton BC, Voigt CA (2012) Genetic programs con-
700 structed from layered logic gates in single cells. *Nature* 491: 249-53.
- 701 52. Wayman JA, Sagar A, Varner JD (2015) Dynamic modeling of cell-free biochemical
702 networks using effective kinetic models. *Processes* 3: 138.
- 703 53. Igel C, Hansen N, Roth S (2007) Covariance matrix adaptation for multi-objective
704 optimization. *Evol Comput* 15: 1-28.
- 705 54. Bezanson J, Edelman A, Karpinski S, Shah VB (2014) Julia: A fresh approach to
706 numerical computing. *CoRR* abs/1411.1607.
- 707 55. Brooks SC, Kazmer S, Levin AA, Yen A (1996) Myeloid differentiation and retinoblas-
708 toma phosphorylation changes in HL-60 cells induced by retinoic acid receptor- and
709 retinoid X receptor-selective retinoic acid analogs. *Blood* 87: 227–237.
- 710 56. Rishi AK, Gerald TM, Shao ZM, Li XS, Baumann RG, et al. (1996) Regulation of the
711 human retinoic acid receptor alpha gene in the estrogen receptor negative human
712 breast carcinoma cell lines skbr-3 and mda-mb-435. *Cancer Res* 56: 5246-52.
- 713 57. Mueller BU, Pabst T, Fos J, Petkovic V, Fey MF, et al. (2006) Atra resolves the dif-
714 ferentiation block in t(15;17) acute myeloid leukemia by restoring pu.1 expression.
715 *Blood* 107: 3330-8.
- 716 58. Luo XM, Ross AC (2006) Retinoic acid exerts dual regulatory actions on the ex-
717 pression and nuclear localization of interferon regulatory factor-1. *Exp Biol Med*

- 718 (Maywood) 231: 619-31.
- 719 59. Sylvester I, Schöler HR (1994) Regulation of the oct-4 gene by nuclear receptors.
720 Nucleic Acids Res 22: 901-11.
- 721 60. Drach J, McQueen T, Engel H, Andreeff M, Robertson KA, et al. (1994) Retinoic
722 acid-induced expression of cd38 antigen in myeloid cells is mediated through
723 retinoic acid receptor-alpha. Cancer Res 54: 1746-52.
- 724 61. Liu M, Iavarone A, Freedman LP (1996) Transcriptional activation of the human
725 p21(waf1/cip1) gene by retinoic acid receptor. correlation with retinoid induction of
726 u937 cell differentiation. J Biol Chem 271: 31723-8.
- 727 62. Bunaciu RP, Yen A (2013) 6-formylindolo (3,2-b)carbazole (ficz) enhances retinoic
728 acid (ra)-induced differentiation of hl-60 myeloblastic leukemia cells. Mol Cancer 12:
729 39.
- 730 63. Balmer JE, Blomhoff R (2002) Gene expression regulation by retinoic acid. J Lipid
731 Res 43: 1773-808.
- 732 64. Rosen ED, Hsu CH, Wang X, Sakai S, Freeman MW, et al. (2002) C/ebpalpha in-
733 duces adipogenesis through ppargamma: a unified pathway. Genes Dev 16: 22-6.
- 734 65. Varley CL, Bacon EJ, Holder JC, Southgate J (2009) Foxa1 and irf-1 intermediary
735 transcriptional regulators of ppargamma-induced urothelial cytodifferentiation. Cell
736 Death Differ 16: 103-14.
- 737 66. Bruemmer D, Yin F, Liu J, Berger JP, Sakai T, et al. (2003) Regulation of the growth
738 arrest and dna damage-inducible gene 45 (gadd45) by peroxisome proliferator-
739 activated receptor gamma in vascular smooth muscle cells. Circ Res 93: e38-47.
- 740 67. Delerive P, De Bosscher K, Besnard S, Vanden Berghe W, Peters JM, et al. (1999)
741 Peroxisome proliferator-activated receptor alpha negatively regulates the vascular
742 inflammatory gene response by negative cross-talk with transcription factors nf-
743 kappaB and ap-1. J Biol Chem 274: 32048-54.

- 744 68. Altioik S, Xu M, Spiegelman BM (1997) Ppargamma induces cell cycle withdrawal:
745 inhibition of e2f/dp dna-binding activity via down-regulation of pp2a. Genes Dev 11:
746 1987-98.
- 747 69. Fei J, Cook C, Gillespie M, Yu B, Fullen K, et al. (2011) Atherogenic ω -6 lipids mod-
748 ulate ppar- egr-1 crosstalk in vascular cells. PPAR Res 2011: 753917.
- 749 70. Song EK, Lee YR, Kim YR, Yeom JH, Yoo CH, et al. (2012) Naadp mediates insulin-
750 stimulated glucose uptake and insulin sensitization by ppar γ in adipocytes. Cell Rep
751 2: 1607-19.
- 752 71. Szanto A, Nagy L (2005) Retinoids potentiate peroxisome proliferator-activated re-
753 ceptor gamma action in differentiation, gene expression, and lipid metabolic pro-
754 cesses in developing myeloid cells. Mol Pharmacol 67: 1935-43.
- 755 72. Han S, Sidell N, Fisher PB, Roman J (2004) Up-regulation of p21 gene expres-
756 sion by peroxisome proliferator-activated receptor gamma in human lung carcinoma
757 cells. Clin Cancer Res 10: 1911-9.
- 758 73. Von Knethen A, Brüne B (2002) Activation of peroxisome proliferator-activated re-
759 ceptor gamma by nitric oxide in monocytes/macrophages down-regulates p47phox
760 and attenuates the respiratory burst. J Immunol 169: 2619-26.
- 761 74. Dispirito JR, Fang B, Wang F, Lazar MA (2013) Pruning of the adipocyte peroxisome
762 proliferator-activated receptor γ cistrome by hematopoietic master regulator pu.1.
763 Mol Cell Biol 33: 3354-64.
- 764 75. Chen H, Ray-Gallet D, Zhang P, Hetherington CJ, Gonzalez DA, et al. (1995) Pu.1
765 (spi-1) autoregulates its expression in myeloid cells. Oncogene 11: 1549-60.
- 766 76. Steidl U, Rosenbauer F, Verhaak RGW, Gu X, Ebralidze A, et al. (2006) Essential
767 role of jun family transcription factors in pu.1 knockdown-induced leukemic stem
768 cells. Nat Genet 38: 1269-77.
- 769 77. Pahl HL, Scheibe RJ, Zhang DE, Chen HM, Galson DL, et al. (1993) The proto-

- 770 oncogene pu.1 regulates expression of the myeloid-specific cd11b promoter. J Biol
771 Chem 268: 5014-20.
- 772 78. Yuki H, Ueno S, Tatetsu H, Niiro H, Iino T, et al. (2013) Pu.1 is a potent tumor
773 suppressor in classical hodgkin lymphoma cells. Blood 121: 962-70.
- 774 79. Li SL, Schlegel W, Valente AJ, Clark RA (1999) Critical flanking sequences of pu.1
775 binding sites in myeloid-specific promoters. J Biol Chem 274: 32453-60.
- 776 80. Timchenko N, Wilson DR, Taylor LR, Abdelsayed S, Wilde M, et al. (1995) Autoreg-
777 ulation of the human c/ebp alpha gene by stimulation of upstream stimulatory factor
778 binding. Mol Cell Biol 15: 1192-202.
- 779 81. Lidonnici MR, Audia A, Soliera AR, Prisco M, Ferrari-Amorotti G, et al. (2010) Ex-
780 pression of the transcriptional repressor gfi-1 is regulated by c/ebpalpha and is
781 involved in its proliferation and colony formation-inhibitory effects in p210bcr/abl-
782 expressing cells. Cancer Res 70: 7949-59.
- 783 82. D'Alo' F, Johansen LM, Nelson EA, Radomska HS, Evans EK, et al. (2003) The
784 amino terminal and e2f interaction domains are critical for c/ebp alpha-mediated
785 induction of granulopoietic development of hematopoietic cells. Blood 102: 3163-
786 71.
- 787 83. Pan Z, Hetherington CJ, Zhang DE (1999) Ccaat/enhancer-binding protein activates
788 the cd14 promoter and mediates transforming growth factor beta signaling in mono-
789 cyte development. J Biol Chem 274: 23242-8.
- 790 84. Harris TE, Albrecht JH, Nakanishi M, Darlington GJ (2001) Ccaat/enhancer-binding
791 protein-alpha cooperates with p21 to inhibit cyclin-dependent kinase-2 activity and
792 induces growth arrest independent of dna binding. J Biol Chem 276: 29200-9.
- 793 85. Bauvois B, Durant L, Laboureau J, Barthélémy E, Rouillard D, et al. (1999) Upreg-
794 ulation of cd38 gene expression in leukemic b cells by interferon types i and ii. J
795 Interferon Cytokine Res 19: 1059-66.

- 796 86. Passioura T, Dolnikov A, Shen S, Symonds G (2005) N-ras-induced growth suppres-
797 sion of myeloid cells is mediated by irf-1. *Cancer Res* 65: 797-804.
- 798 87. Dahl R, Iyer SR, Owens KS, Cuylear DD, Simon MC (2007) The transcriptional
799 repressor gfi-1 antagonizes pu.1 activity through protein-protein interaction. *J Biol
800 Chem* 282: 6473-83.
- 801 88. Duan Z, Horwitz M (2003) Targets of the transcriptional repressor oncoprotein gfi-1.
802 *Proc Natl Acad Sci U S A* 100: 5932-7.
- 803 89. Chen H, Zhang P, Radomska HS, Hetherington CJ, Zhang DE, et al. (1996) Octamer
804 binding factors and their coactivator can activate the murine pu.1 (spi-1) promoter.
805 *J Biol Chem* 271: 15743-52.
- 806 90. Behre G, Whitmarsh AJ, Coghlan MP, Hoang T, Carpenter CL, et al. (1999) c-jun
807 is a jnk-independent coactivator of the pu.1 transcription factor. *J Biol Chem* 274:
808 4939-46.
- 809 91. Kardassis D, Papakosta P, Pardali K, Moustakas A (1999) c-jun transactivates the
810 promoter of the human p21(waf1/cip1) gene by acting as a superactivator of the
811 ubiquitous transcription factor sp1. *J Biol Chem* 274: 29572-81.
- 812 92. Johnson DG, Ohtani K, Nevins JR (1994) Autoregulatory control of e2f1 expression
813 in response to positive and negative regulators of cell cycle progression. *Genes Dev*
814 8: 1514-25.
- 815 93. Fu M, Zhang J, Lin Y, Zhu X, Ehrengruber MU, et al. (2002) Early growth response
816 factor-1 is a critical transcriptional mediator of peroxisome proliferator-activated
817 receptor-gamma 1 gene expression in human aortic smooth muscle cells. *J Biol
818 Chem* 277: 26808-14.
- 819 94. Mak KS, Funnell APW, Pearson RCM, Crossley M (2011) Pu.1 and haematopoietic
820 cell fate: Dosage matters. *Int J Cell Biol* 2011: 808524.
- 821 95. Chen F, Wang Q, Wang X, Studzinski GP (2004) Up-regulation of egr1 by 1,25-

- 822 dihydroxyvitamin d3 contributes to increased expression of p35 activator of cyclin-
823 dependent kinase 5 and consequent onset of the terminal phase of hl60 cell differ-
824 entiation. *Cancer Res* 64: 5425-33.
- 825 96. Suh J, Jeon YJ, Kim HM, Kang JS, Kaminski NE, et al. (2002) Aryl hydrocarbon
826 receptor-dependent inhibition of ap-1 activity by 2,3,7,8-tetrachlorodibenzo-p-dioxin
827 in activated b cells. *Toxicol Appl Pharmacol* 181: 116-23.
- 828 97. Shen M, Bunaciu RP, Congleton J, Jensen HA, Sayam LG, et al. (2011) Inter-
829 feron regulatory factor-1 binds c-cbl, enhances mitogen activated protein kinase
830 signaling and promotes retinoic acid-induced differentiation of hl-60 human myelo-
831 monoblastic leukemia cells. *Leuk Lymphoma* 52: 2372-9.
- 832 98. Bunaciu RP, Yen A (2011) Activation of the aryl hydrocarbon receptor ahr promotes
833 retinoic acid-induced differentiation of myeloblastic leukemia cells by restricting ex-
834 pression of the stem cell transcription factor oct4. *Cancer Res* 71: 2371-80.
- 835 99. Jackson DA, Pombo A, Iborra F (2000) The balance sheet for transcription: an anal-
836 ysis of nuclear rna metabolism in mammalian cells. *FASEB J* 14: 242-54.
- 837 100. Zhao ZW, Roy R, Gebhardt JCM, Suter DM, Chapman AR, et al. (2014) Spatial orga-
838 nization of rna polymerase ii inside a mammalian cell nucleus revealed by reflected
839 light-sheet superresolution microscopy. *Proc Natl Acad Sci U S A* 111: 681-6.
- 840 101. Freitas R, Merkle R (2004) Kinematic Self-Replicating Machines. Oxford University
841 Press.
- 842 102. Yang E, van Nimwegen E, Zavolan M, Rajewsky N, Schroeder M, et al. (2003) De-
843 cay rates of human mrnas: correlation with functional characteristics and sequence
844 attributes. *Genome Res* 13: 1863-72.
- 845 103. Doherty MK, Hammond DE, Clague MJ, Gaskell SJ, Beynon RJ (2009) Turnover
846 of the human proteome: determination of protein intracellular stability by dynamic
847 silac. *J Proteome Res* 8: 104-12.

- 848 104. Darzacq X, Shav-Tal Y, de Turris V, Brody Y, Shenoy SM, et al. (2007) In vivo dy-
849 namics of rna polymerase ii transcription. Nat Struct Mol Biol 14: 796-806.
- 850 105. Boström K, Wettsten M, Borén J, Bondjers G, Wiklund O, et al. (1986) Pulse-chase
851 studies of the synthesis and intracellular transport of apolipoprotein b-100 in hep g2
852 cells. J Biol Chem 261: 13800-6.
- 853 106. Meyers R, editor (2004) Encyclopedia of Molecular Cell Biology and Molecular
854 Medicine, Volume 1, 2nd Edition. ISBN: 978-3-527-30543-8. Wiley-Blackwell.
- 855 107. Rosenbluth MJ, Lam WA, Fletcher DA (2006) Force microscopy of nonadherent
856 cells: a comparison of leukemia cell deformability. Biophys J 90: 2994-3003.

Table 1: Myelomonocytic transcription factor connectivity used in the signal integration and phenotype modules.

857

858

Effector	Effect	Target	Source
RAR α	+	RAR α	(56)
	+	PU.1	(57)
	+	C/EBP α	(36)
	+	IRF-1	(58)
	-	Oct4	(59)
	+	CD38	(60)
	+	p21	(61)
	+	AhR	(62)
	+	EGR1	(63)
PPAR γ	+	C/EBP α	(64)
	+	IRF-1	(65)
	+	Oct1	(66)
	-	AP-1	(67)
	-	E2F	(68)
	-	EGR1	(69)
	+	CD38	(70)
	+	CD14	(71)
	+	p21	(72)
	-	p47phox	(73)
PU.1	-	PPAR γ	(74)
	+	PU.1	(75)
	+	AP-1	(76)
	+	EGR1	(32)
	+	CD11b	(77)
	+	p21	(78)
	+	p47phox	(79)
C/EBP α	+	PPAR γ	(64)
	+	PU.1	(37)
	+	C/EBP α	(80)
	+	Gfi-1	(81)
	-	E2F	(82)
	+	CD14	(83)

	+	p21	(84)
IRF-1	+	CD38	(85)
	+	p21	(86)
	-	PU.1	(87)
	-	C/EBP α	(88)
	-	E2F	(88)
	-	EGR1	(32)
	-	p21	(88)
Oct1	+	PU.1	(89)
AP-1	-	PPAR γ	(67)
	+	PU.1	(90)
	+	p21	(91)
E2F	+	E2F	(92)
EGR1	+	PPAR γ	(93)
	-	Gfi-1	(94)
	+	CD14	(95)
AhR	+	AP-1	(96)
	+	IRF-1	(97)
	-	Oct4	(98)
	-	PU.1	

Table 2: Characteristic model parameters estimated from literature.

Symbol	Description	Value	Units	Source
R_1	RNA polymerase abundance	75,000	copies/cell	(99, 100)
R_2	Ribosome abundance	1×10^6	copies/cell	(101)
G_i	Characteristic gene abundance	2	copies/cell	this study
K_X	Saturation constant transcription	4,600	copies/cell	this study
K_T	Saturation constant translation	100,000	copies/cell	this study
$t_{1/2,m}$	characteristic mRNA half-life (transcription factor)	2	hr	(102)
$t_{1/2,p}$	characteristic protein half-life	10	hr	(103)
$\theta_{m,j}$	characteristic mRNA degradation constant	0.34	hr^{-1}	derived
$\theta_{p,j}$	characteristic protein degradation constant	0.07	hr^{-1}	derived
861				
t_d	HL-60 doubling time	19.5	hr	this study
μ	growth rate	0.035	hr^{-1}	derived
k_d	death rate	0.10μ	hr^{-1}	derived
e_T	elongation rate RNA polymerase	6	nt/s	(104)
e_X	elongation rate Ribosome	5	aa/s	(105)
$L_{T,o}$	characteristic gene length	15,000	nt	(106)
$L_{X,o}$	characteristic transcript length	5,000	nt	derived
k_T	characteristic transcription rate	1.44	hr^{-1}	derived
k_X	characteristic translation rate	3.60	hr^{-1}	derived
D	Diameter of an HL-60 cell	12.4	μm^3	(107)
f_C	cytoplasmic fraction	0.51	dimensionless	(107)

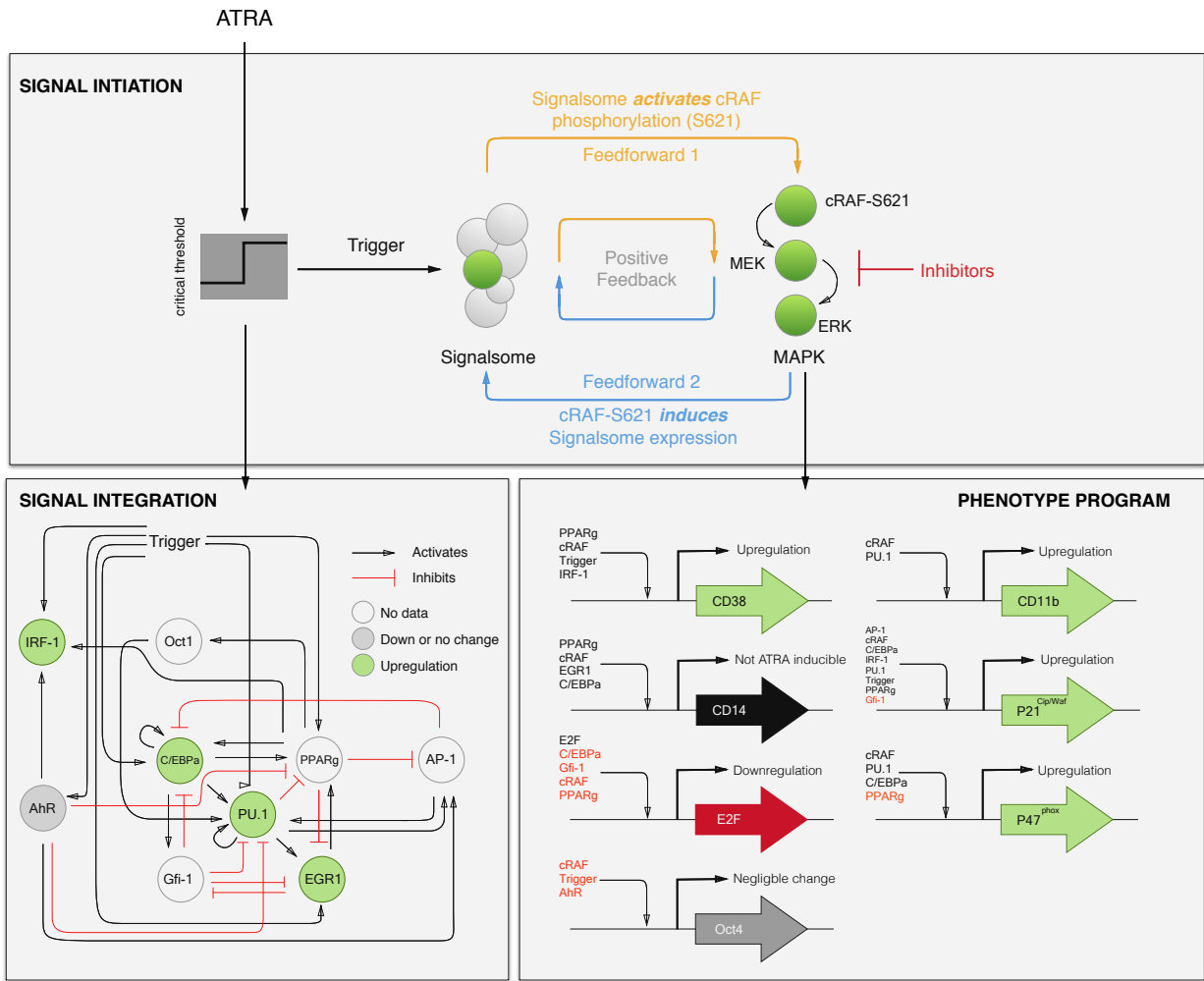


Fig. 1: Schematic of the effective ATRA differentiation circuit. Above a critical threshold, ATRA activates an upstream Trigger, which induces signalsome complex formation. Signalsome activates the mitogen-activated protein kinase (MAPK) cascade which in turn drives the differentiation program and signalsome formation. Both Trigger and activated cRaf-pS621 drive a phenotype gene expression program responsible for differentiation. Trigger activates the expression of a series of transcription factors which in combination with cRaf-pS621 result in phenotypic change.

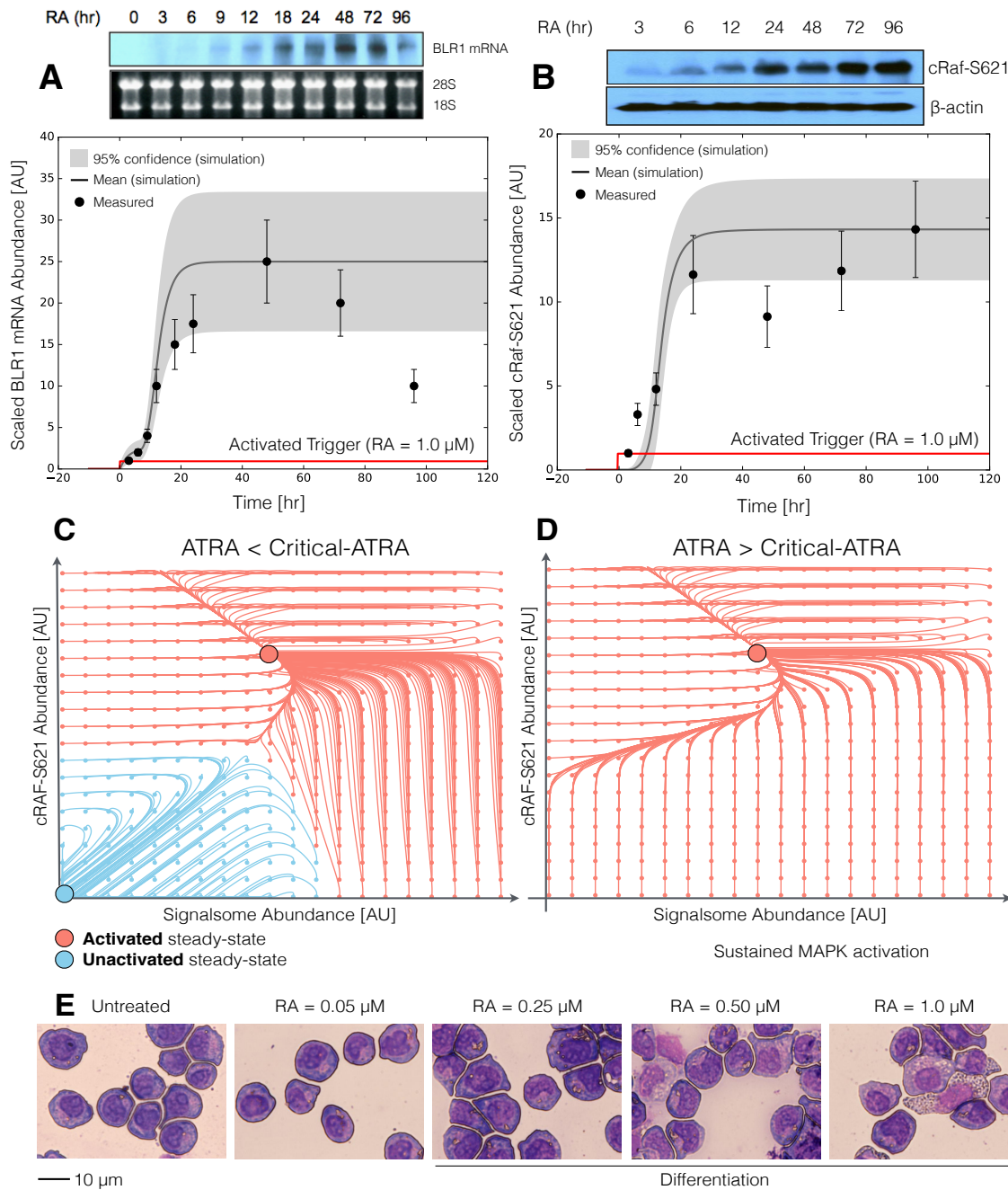


Fig. 2: Model analysis for ATRA-induced HL-60 differentiation. A: BLR1 mRNA versus time following exposure to 1 μ M ATRA at $t = 0$ hr. B: cRaf-pS621 versus time following exposure to 1 μ M ATRA at $t = 0$ hr. Points denote experimental measurements, solid lines denote the mean model performance. Shaded regions denote the 99% confidence interval calculated over the parameter ensemble. C: Signalsome and cRaf-pS621 nullclines for ATRA below the critical threshold. The model had two stable steady states and a single unstable state in this regime. D: Signalsome and cRaf-pS621 nullclines for ATRA above the critical threshold. In this regime the model had only a single stable steady state. E: Morphology of HL-60 as a function of ATRA concentration ($t = 72$ hr).

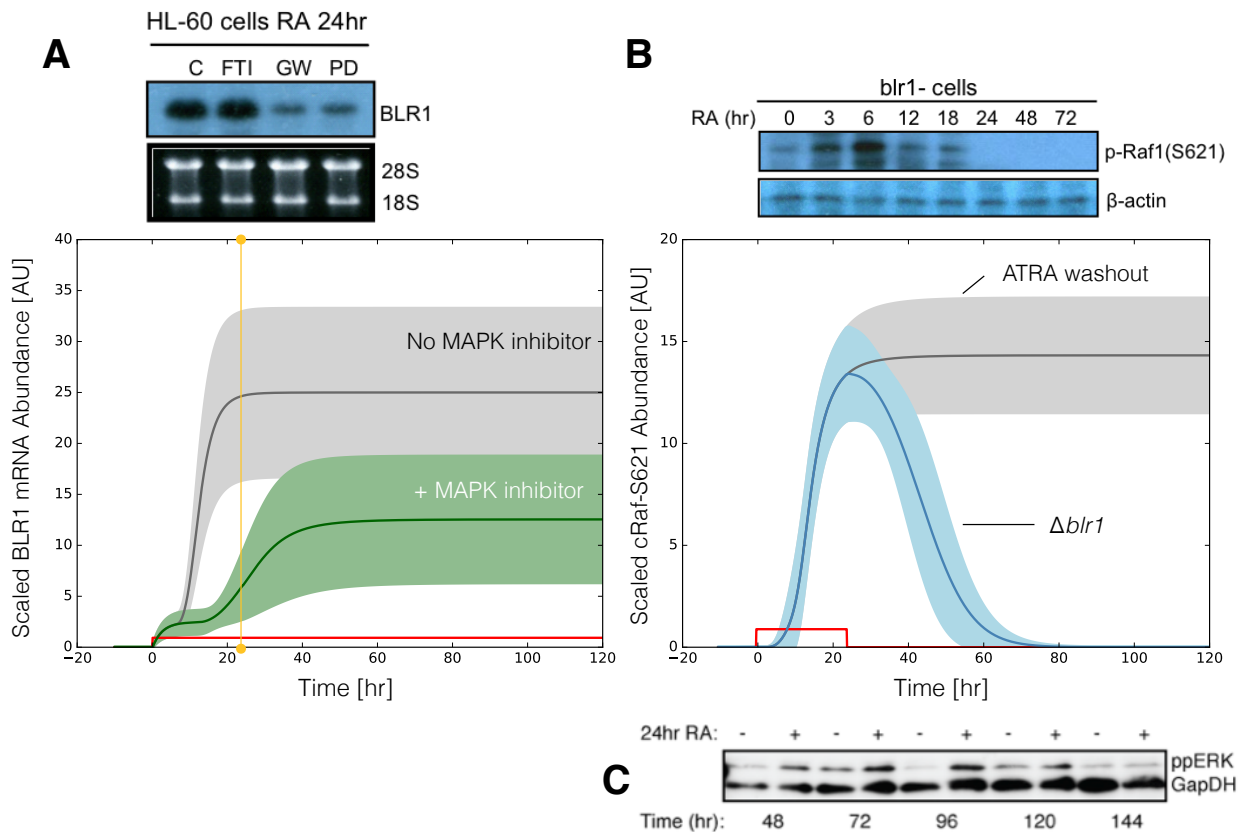


Fig. 3: Model simulation following exposure to $1\mu\text{M}$ ATRA. A: BLR1 mRNA versus time with and without MAPK inhibitor. B: cRaf-pS621 versus time following pulsed exposure to $1\mu\text{M}$ ATRA with and without BLR1. Solid lines denote the mean model performance, while shaded regions denote the 99% confidence interval calculated over the parameter ensemble. C: Western blot analysis of phosphorylated ERK1/2 in ATRA washout experiments. Experimental data in panels A and B were reproduced from Wang and Yen (20), data in panel C is reported in this study.

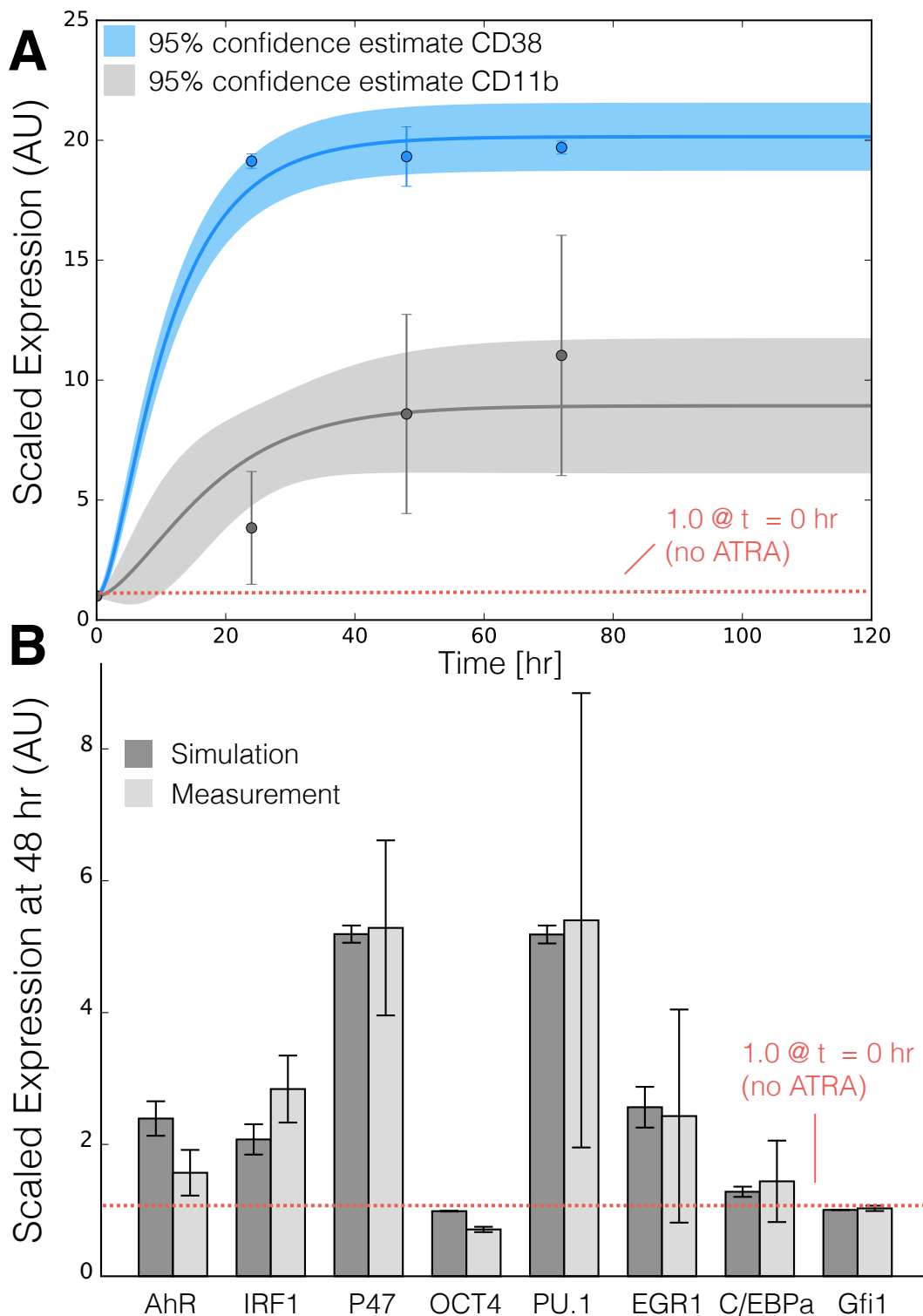


Fig. 4: Model simulation of the HL-60 gene expression program following exposure to $1\mu\text{M}$ ATRA at $t = 0$ hr. A: CD38 and CD11b expression versus time following ATRA exposure at time $t = 0$ hr. B: Gene expression at $t = 48$ hr following ATRA exposure. Experimental data in panels A and B were reproduced from Jensen et al. (25).

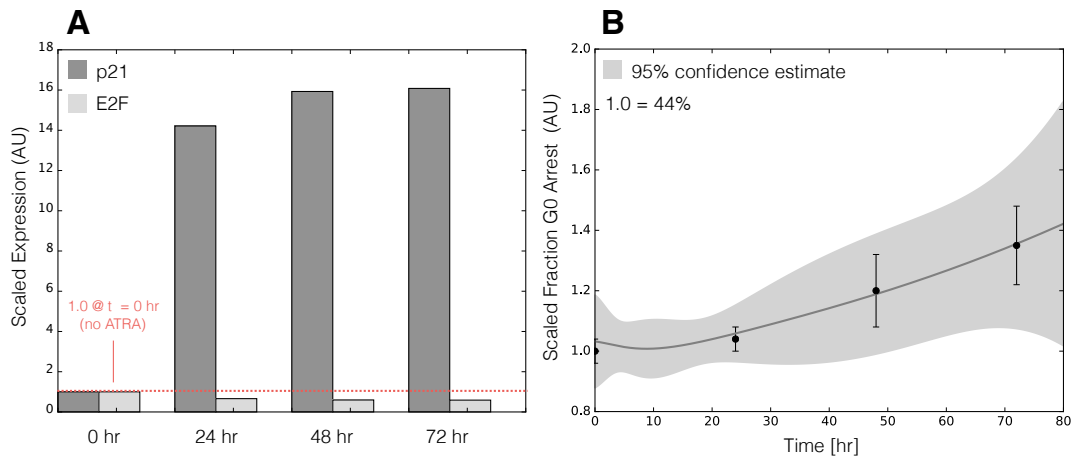


Fig. 5: Model simulation of HL-60 cell-cycle arrest following exposure to $1\mu\text{M}$ ATRA at $t = 0$ hr. A: Predicted p21 and E2F expression levels for the best parameter set following ATRA exposure at time $t = 0$ hr. B: Estimated fraction of HL-60 cells in G0 arrest following ATRA exposure at time $t = 0$ hr. The gray region denotes the 95% confidence estimate of the polynomial model. Experimental data in panel B was reproduced from Jensen et al. (25).

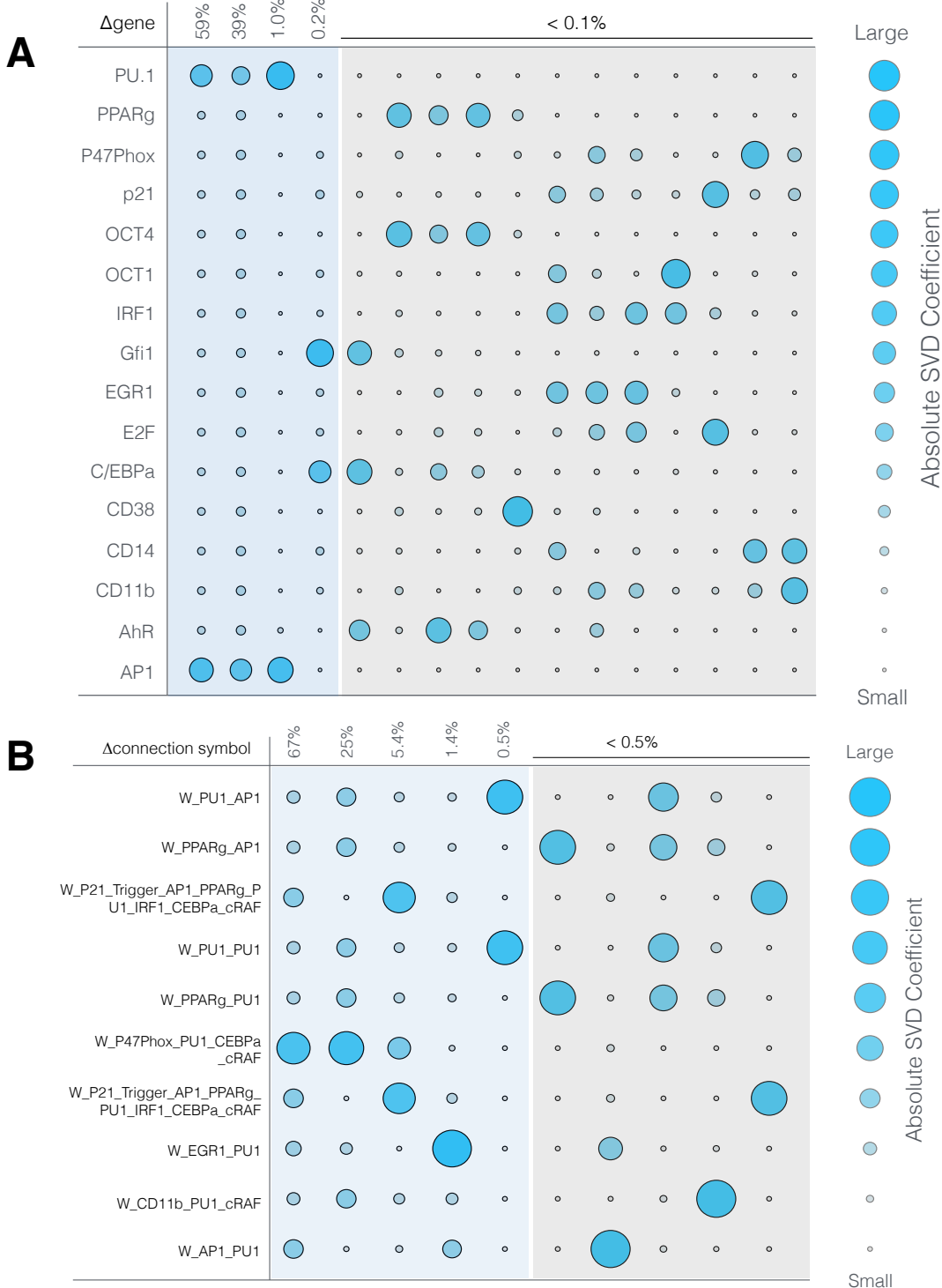


Fig. 6: Robustness of the HL-60 differentiation program following exposure to $1\mu\text{M}$ ATRA at $t = 0$ hr. A: Singular value decomposition of the system response (l^2 -norm between the perturbed and nominal state) following pairwise gene knockout simulations using the best fit parameter set. The percentage at the top of each column describes the fraction of the variance in the system state captured by the node combinations in the rows. B: Singular value decomposition of the system response (l^2 -norm between the perturbed and nominal state) following the pairwise removal of connections from the PU.1 and AP1 nodes.

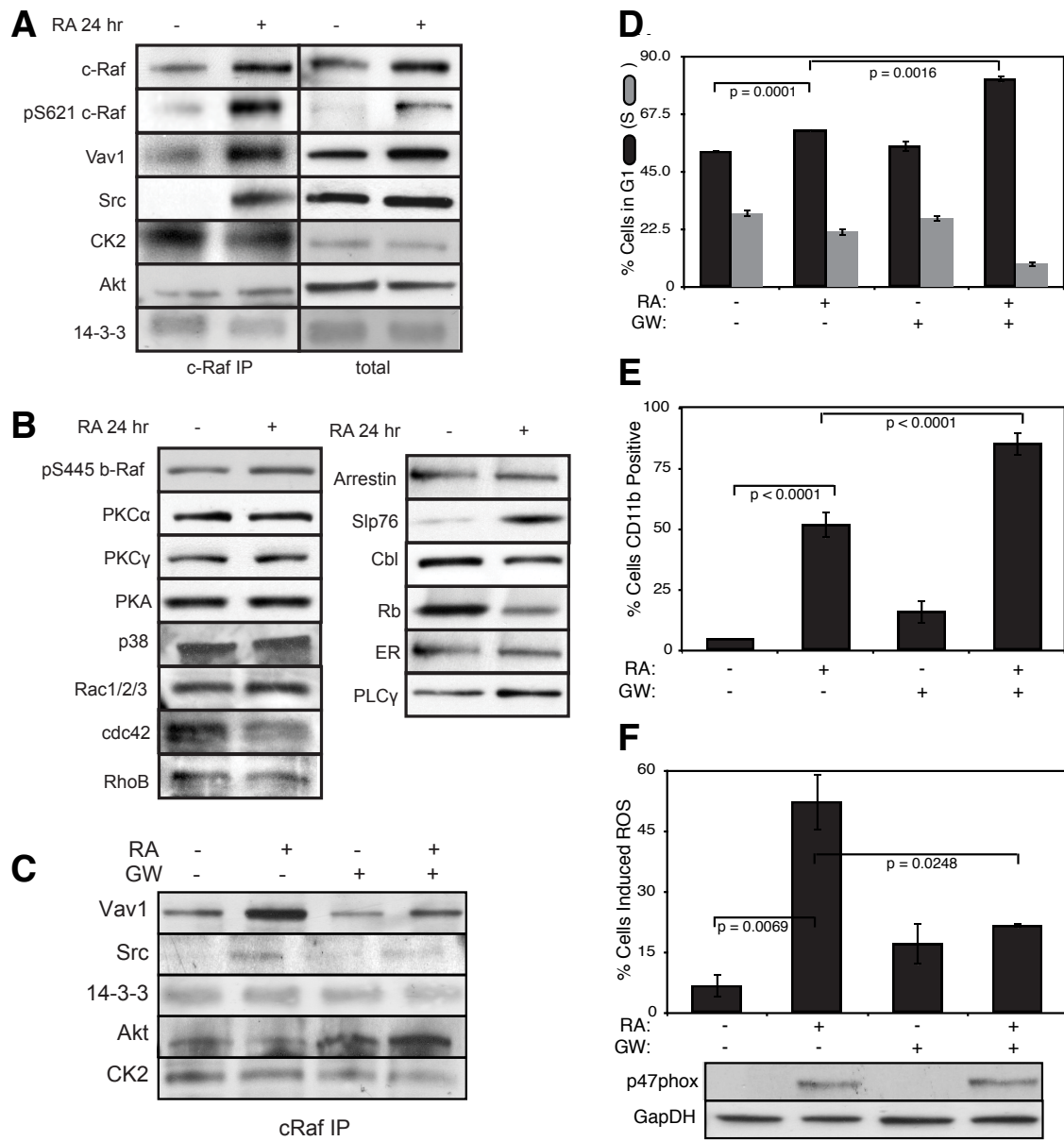


Fig. 7: Investigation of a panel of possible Raf interaction partners in the presence and absence of ATRA. A: Species identified to precipitate out with Raf: first column shows Western blot analysis on total Raf immunoprecipitation with and without 24 hr ATRA treatment and the second on total lysate. B: The expression of species considered that did not precipitate out with Raf at levels detectable by Western blot analysis on total lysate. C: Effect of the Raf inhibitor GW5074 on Raf interactions as determined by Western blot analysis of total Raf immunoprecipitation. The Authors note the signal associated with Src was found to be weak. D: Cell Cycle distribution as determined by flow cytometry indicated arrest induced by ATRA, which was increased by the addition of GW5074. E: Expression of the cell surface marker CD11b as determined by flow cytometry indicated increased expression induced by ATRA, which was enhanced by the addition of GW5074. F: Inducible reactive oxygen species (ROS) as determined by DCF flow cytometry. The functional differentiation response of ATRA treated cells was mitigated by GW5074.